nature ecology & evolution

ARTICLES

https://doi.org/10.1038/s41559-019-0834-1

OPEN

Megaphylogeny resolves global patterns of mushroom evolution

Torda Varga[1], Krisztina Krizsán[1], Csenge Földi[1], Bálint Dima[2], Marisol Sánchez-García[3], Santiago Sánchez-Ramírez[4], Gergely J. Szöllősi[5], János G. Szarkándi[6], Viktor Papp[7], László Albert[8], William Andreopoulos[9], Claudio Angelini[10,11], Vladimír Antonín[12], Kerrie W. Barry[9], Neale L. Bougher[13], Peter Buchanan[14], Bart Buyck[15], Viktória Bense[1], Pam Catcheside[16], Mansi Chovatia[9], Jerry Cooper[17], Wolfgang Dämon[18], Dennis Desjardin[19], Péter Finy[20], József Geml[21], Sajeet Haridas[9], Karen Hughes[22], Alfredo Justo[3], Dariusz Karasiński[23], Ivona Kautmanova[24], Brigitta Kiss[1], Sándor Kocsubé[6], Heikki Kotiranta[25], Kurt M. LaButti[9], Bernardo E. Lechner[26], Kare Liimatainen[27], Anna Lipzen[9], Zoltán Lukács[28], Sirma Mihaltcheva[9], Louis N. Morgado[21,41], Tuula Niskanen[27], Machiel E. Noordeloos[21], Robin A. Ohm[29], Beatriz Ortiz-Santana[30], Clark Ovrebo[31], Nikolett Rácz[6], Robert Riley[9], Anton Savchenko[32,42], Anton Shiryaev[33], Karl Soop[34], Viacheslav Spirin[32], Csilla Szebenyi[6,43], Michal Tomšovský[35], Rodham E. Tulloss[36,37], Jessie Uehling[38], Igor V. Grigoriev[9,39], Csaba Vágvölgyi[6], Tamás Papp[6,43], Francis M. Martin[40], Otto Miettinen[32], David S. Hibbett[3] and László G. Nagy[1*]

Mushroom-forming fungi (Agaricomycetes) have the greatest morphological diversity and complexity of any group of fungi. They have radiated into most niches and fulfil diverse roles in the ecosystem, including wood decomposers, pathogens or mycorrhizal mutualists. Despite the importance of mushroom-forming fungi, large-scale patterns of their evolutionary history are poorly known, in part due to the lack of a comprehensive and dated molecular phylogeny. Here, using multigene and genome-based data, we assemble a 5,284-species phylogenetic tree and infer ages and broad patterns of speciation/extinction and morphological innovation in mushroom-forming fungi. Agaricomycetes started a rapid class-wide radiation in the Jurassic, coinciding with the spread of (sub)tropical coniferous forests and a warming climate. A possible mass extinction, several clade-specific adaptive radiations and morphological diversification of fruiting bodies followed during the Cretaceous and the Paleogene, convergently giving rise to the classic toadstool morphology, with a cap, stalk and gills (pileate-stipitate morphology). This morphology is associated with increased rates of lineage diversification, suggesting it represents a key innovation in the evolution of mushroom-forming fungi. The increase in mushroom diversity started during the Mesozoic-Cenozoic radiation event, an era of humid climate when terrestrial communities dominated by gymnosperms and reptiles were also expanding.

Explosive diversification events, with intermittent periods of relatively little change, have generated uneven patterns of species richness across the tree of life. Although rapid radiations have been inferred in many clades[1–5], few examples exist for fungi, in part because of their limited fossil record, and the lack of comprehensive phylogenies. Advances in modelling the evolutionary process now allow such inferences to be made from phylogenetic trees. Studies of diversification of mushroom-forming fungi have focused on individual clades[6–9], yielding hypotheses on ecological opportunities[6], the evolution of mutualistic lifestyle[7,10] and fruiting body morphologies[6,11] as drivers of adaptive evolution in fungi. However, these inferences, based on specific clades, remained untested across larger phylogenetic scales. Fruiting bodies provide support and protection for developing spores, which probably represents a driving force for increasingly more efficient morphologies[12]. Ancestral fruiting bodies of the Agaricomycotina were probably crust-like, 'resupinate' forms[13,14], which then evolved into increasingly more complex forms, including derived 'pileate-stipitate' types, which are differentiated into a cap, stipe and hymenophore (spore-bearing surface). Pileate-stipitate forms have arisen repeatedly from simpler morphologies (for example, resupinate or coral-like) during evolution[12,13,15] and dominate extant agaricomycete diversity (>21,000 described species[16]), but how this diversity arose, what explains the dominance of pileate-stipitate species in the class and whether fruiting body morphology impacts diversification rates (for example, as a key innovation) are not known.

Results and discussion

We investigated broad patterns of diversification in Agaricomycetes using a phylogenetic comparative approach and generated a highly comprehensive phylogeny of the group, comprising 5,284 species (Fig. 1). Our dataset represents around 26% of described Agaricomycetes, a notably high sampling density for any fungal group. Our inferences of phylogenetic trees combine a robust

A full list of affiliations appears at the end of the paper.

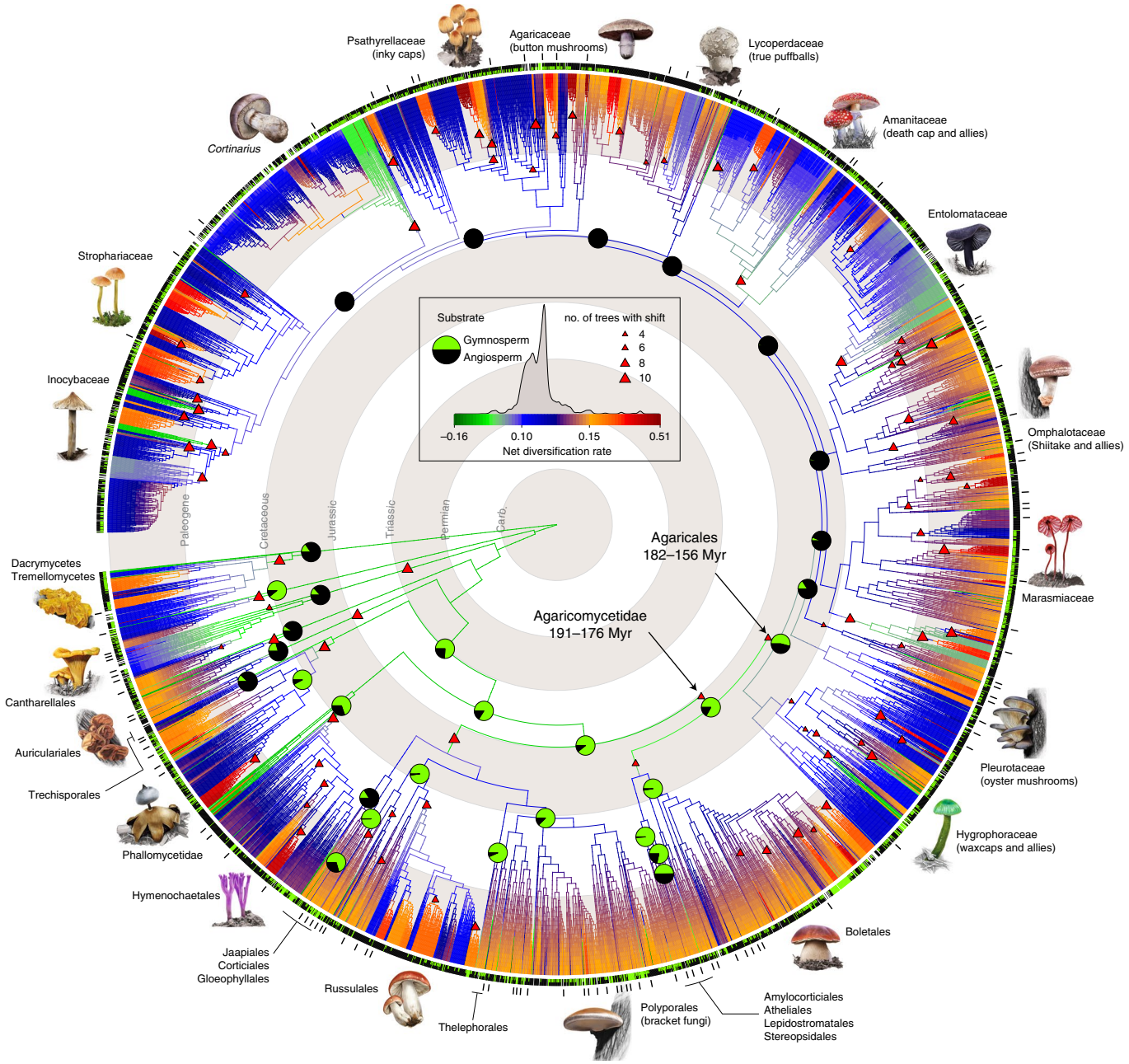

Fig. 1 | Phylogenetic relationships and diversification across 5,284 mushroom-forming fungi. One of the 245 analysed maximum-likelihood trees was randomly chosen and visualized. Trees were inferred from nrLSU, *rpb2, ef1-a* sequences with a phylogenomic backbone constraint of deep nodes. Branches are coloured by net diversification (speciation minus extinction) rate inferred in Bayesian Analysis of Macroevolutionary Mixtures (BAMM). Warmer colours denote a higher rate of diversification. Significant shifts in diversification rate are shown by triangles at nodes. Only shifts present on >50% of ten trees, with a Bayesian posterior probability >0.5 and a posterior odds ratio >5 are shown. See Supplementary Data 6 for detailed discussion of shifts. Reconstructed probabilities of ancestral plant hosts for order-level clades are shown as pie charts partitioned by the inferred ancestral probability for gymnosperm (green) and angiosperm host (black). Pie charts are given for the most recent common ancestors of each order plus backbone nodes within the Agaricales—for small orders see Supplementary Data 3. Inner and outer bars around the tree denote extant substrate preference (black, angiosperm; green, gymnosperm; grey, generalist) and the placement of species used for inferring the 650-gene phylogenomic backbone phylogeny. Geological time scale is indicated with grey/white concentric rings.

genome-based backbone phylogeny of 104 species (650 genes, 141,951 amino acid characters, see Supplementary Figs. 1–3, Supplementary Table 1 and Supplementary Notes 1 and 2) with sequence data from up to three nuclear loci for 5,284 taxa (large subunit (LSU) rRNA, rpb2, ef-1a, 5,737 characters). New sequence data were generated for 1,222 species (Supplementary Note 2 and Supplementary Data 1), including nine new genomes of phylogenetically key taxa (Supplementary Note 3). The phylogenetic tree topology is largely congruent with previously published clade-specific phylogenies and resolves 21 orders of Agaricomycetes plus Dacrymycetes and Tremellomycetes as outgroups. Most of the nodes received strong bootstrap support, but we also identified nodes that require more scrutiny and probably denser taxon sampling to be resolved with certainty (for a detailed genome-based

overview of agaricomycete phylogeny, see Supplementary Note 1). We inferred ten time-calibrated phylogenies for the 5,284 taxa dataset using a two-stage Bayesian approach and all taxonomically informative, non-conflicting fossil calibration points available in the Agaricomycetes (eight fossils, determined by a fossil cross-validation procedure, see Supplementary Fig. 4, Supplementary Table 2 and Supplementary Note 4). Inferred node heights of the order-level clades range from 183 to 71 Myr, which places the origin of most order-level clades in the Jurassic, with the Cantharellales (mean age: 184 Myr, 144–261 Myr across ten chronograms), Agaricales (mean: 173 Myr, 160–182 Myr), Hymenochaetales (mean: 167 Myr, 130–180 Myr) and Boletales (mean: 142 Myr, 133–153 Myr) being the oldest. The Agaricomycetidae, the group uniting the Agaricales and Boletales was estimated at ~185 Myr (174–192 Myr, Fig. 1 and Supplementary Note 4). Because these molecular clock estimates are older than previous phylogenomics-based figures[17–19], we performed sensitivity analyses to address the underlying causes, which suggest that the differences are attributable to the higher taxon sampling density in both our genome-based and 5,284-species tree and not to differences in software or choice of priors in fossil-based molecular clock calibrations. Various taxon and fossil sampling schemes, tree (5,284-taxon versus the genome-based phylogeny) and software choice had little effect on inferred ages (Supplementary Data 2 and Supplementary Note 4), providing a robust set of age estimates for Agaricomycetes.

We analysed global rates of speciation and extinction in a macroevolutionary framework using BAMM[20]. We accounted for incomplete and unequal sampling by using clade-specific sampling fractions and by ensuring that each genus was sampled in proportion to the number of its described species. Analyses of diversification rates in ten time-calibrated phylogenies provided evidence for rate variation through time and across lineages. Diversification rates increased abruptly at ~180 Myr ago in the early Jurassic (Fig. 2), coinciding with the breakup of Pangea, the onset of a warm, humid climate and the spread of (sub)tropical gymnosperm forests. Consistent with this, ancestral state reconstructions suggest that the last common ancestors of most orders were likely associated with gymnosperms as hosts (Figs. 1 and 3a, Supplementary Data 3 and Supplementary Note 5), followed by multiple shifts to and diversification in association with angiosperms as hosts during the Cretaceous, similar to patterns observed in a radiation of herbivorous beetles[21]. This agrees with observations of fungus-plant coevolution at smaller scales[10,22], frequent host switches during fungal evolution[23] and might reflect the dependence of fungi on plants as nutrient sources or mutualistic partners.

Acceleration of speciation is observed across all larger orders (Supplementary Data 4), suggestive of an external underlying cause, such as climate change or nutrient availability, instead of clade-specific events. We find that the rise in speciation rates in the Jurassic is coupled with a slightly delayed increase in extinction rates ~150 Myr ago (Fig. 2). Although estimating extinction rates from phylogenies is notoriously difficult[24–26], this signal is also detected in an independent analysis using an episodic speciation/extinction model[27] under a variety of conditions (Supplementary Note 6, Supplementary Fig. 6 and Supplementary Tables 3 and 4). Together, these data suggest that fungi experienced severe extinction in a period that falls close to a mass extinction event at the Jurassic/Cretaceous boundary[28], an era with a fluctuating edaphic conditions, differential extinction of several metazoan groups, and a relatively stable flora. On the other hand, we find no evidence for increased probability of extinction around the Cretaceous/Tertiary boundary, a period of severe mass extinction in plant and animal lineages. It has been hypothesized that the massive deforestation after the bolide impact has buffered fungi through the period[29], which is supported by a peak in fungal spore and hyphae fossilization right after the cataclysm[30] and would explain the lack of mass extinction signal in our data.

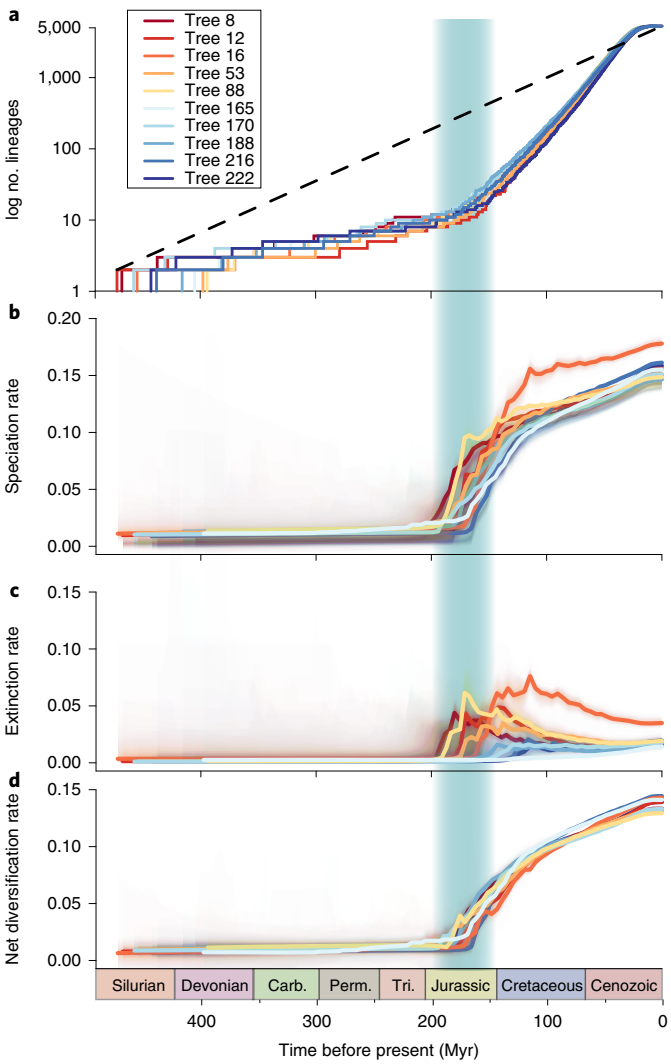

Fig. 2 | Patterns of diversification of mushroom-forming fungi through time. a–d, Lineages through time plot, **a**, showing the log number of lineages through time; **b,** speciation rate; **c**, extinction rate and **d**, net diversification rate through geologic time estimated using BAMM on ten chronograms comprising 5,284-species. 95% confidence intervals of rate estimates are shown by shaded areas. The Jurassic period is shaded in green. Carb., Carboniferous; Perm., Permian and Tri., Triassic.

The latitudinal diversity gradient (LDG) hypothesis posits that species richness increases from the poles towards the tropics. To test if this general prediction is valid for Agaricomycetes, we analysed latitude-dependent diversification rates across all 4,429 species for which sufficient geographic data could be obtained (see Methods). Agaricomycetes display their highest species diversity and net diversification rates in the temperate zone (Supplementary Figs. 7 and 8, Supplementary Tables 5 and 6 and Supplementary Note 7), which contrasts with the diversity gradient from the poles towards the tropics in animals and plants[31]. Although such a pattern could arise as a result of more concentrated efforts of recording fungi in the temperate zone, we find that the zone with highest speciation rate (between 20 and 40° in the temperate zone) does not coincide with the zone of the highest sampling density (30–60°) in our data. This suggests that our inference of a temperate peak in diversification rates is largely independent from sampling density. A reversed LDG has already been implied for major fun-

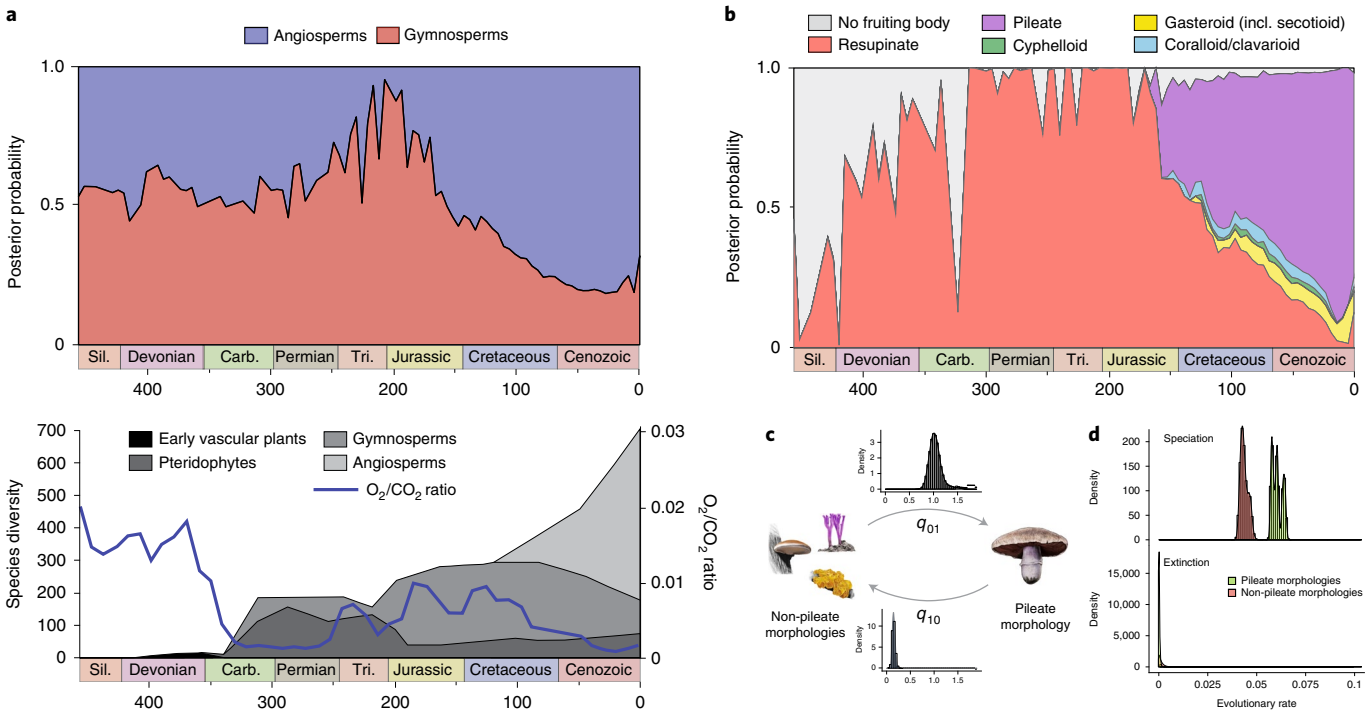

Fig. 3 | The evolution of morphological and nutritional traits of mushrooms through time. a, The evolution of substrate association through geologic time (top) and the evolution of vascular plant diversity and O_2/CO_2 levels (bottom, adapted from Niklas[41] and Berner[42]. Inferred ancestral probabilities of fruiting body types were summarized across the ten phylogenies, by splitting the time scale of each tree into 100 bins and summing probabilities across the tree. **b**, The evolution of fruiting body types through time and the radiation of the agaricoid morphology since the Jurassic. Plot created as in **a**. For details of character coding and ancestral state reconstructions and detailed results, see Supplementary Note 5. **c**, Schematic model of the evolution of pileate-stipitate morphologies. The posterior distribution of transition rates from non-pileate (left) towards pileate-stipitate forms (right) and vice versa are shown above the arrows. Rates were estimated by Markov chain Monte Carlo (MCMC) in BayesTraits. **d**, Posterior distribution of trait-dependent speciation and extinction rates estimated under the binary state speciation and extinction (BiSSE) model for non-pileate versus pileate-stipitate fruiting body morphologies. Carb., Carboniferous; Perm., Permian and Tri., Triassic.

gal groups by several surveys of environmental sequences[32–34] and phylogenetic analyses[22,35], in particular for ectomycorrhizal fungi. Although such signals might also be sensitive to biased taxonomic efforts across ecoregions, these data suggest that Agaricomycetes might not conform to broad macroecological patterns that dominate in animal and plant lineages.

To obtain a more resolved picture on diversification histories, we analysed rate variation across clades. We identified 85 significant shifts in diversification rate (defined as shifts present in ≥50% of trees with marginal odds ratio ≥5) that included clades of diverse ages spread out across the Agaricomycetes (Fig. 1, Supplementary Data 5, Supplementary Figs. 9 and 10, Supplementary Tables 7 and 8 and Supplementary Note 8). The largest of these comprises the Agaricomycetidae, consistent with results of rate through time and lineages through time analyses, which revealed an acceleration of net diversification rates in the Jurassic (Fig. 2). Order-level shifts to higher diversification rates were inferred in the last common ancestor of the Auriculariales; that of the Cantharellales, the Hymenochaetales (excluding the Repetobasidiaceae), the Russulales and the Agaricales (excluding the hygrophoroid and pleurotoid clades (sensu Matheny[15]) (Fig. 1). Most of the shifts (67%) were found in the Agaricales and predominantly in the Paleogene, consistent with a dynamic evolutionary history of the order but also with its largest share of diversity in the class. We found accelerated diversification in the genera *Coprinellus* and *Laccaria*, as reported previously[6,7], but also in *Cortinarius*, *Amanita* and *Lepiota*, among others (for the complete list of shifts see Supplementary Data 5). Some of these represent the most taxonomically diverse agaric genera, such as *Cortinarius* with >2,000 (ref. [16]) species described. Accelerated diversification in these groups is consistent with patterns seen in adaptive radiations[36,37]. Indeed, many clades show a diversification slowdown through time, a key sign of adaptive radiations[36] (Supplementary Data 6), suggesting that many of the detected shifts may feature rapid adaptive filling of available niches. Among the 85 detected shifts in diversification rates, there were several that denoted old clades with low diversity, in which the shift represents a diversification slowdown rather than acceleration. For example, the genus *Typhula*, comprising species with minute club-shaped fruiting bodies, is an ancient group (dated at around 76 Myr) with a low diversity and an inferred diversification slowdown along its stem branch. Such parameters may indicate clades of relict lineages rooting deeply in Agaricales history but having only a few extant representatives. Taken together, these analyses provide a global view on bursts and slowdowns in the diversification history of mushroom-forming fungi and should facilitate a better understanding of adaptive diversification events in fungi, of which only a single example has been explicitly demonstrated[6].

We next asked how morphological innovations may have contributed to shape the extant diversity of Agaricomycetes. Because fruiting body complexity is an important adaptive trait[13,14], we mapped the evolution of fruiting body morphologies on the phylogeny and examined its impact on diversification rates. We performed ancestral state reconstructions and summarized inferred ancestral states through time across ten chronograms (Fig. 3b). In line with previous studies[13,14], our reconstructions suggest ancestors

with resupinate (crust-like) fruiting bodies for most early nodes along the backbone of the Agaricomycetes. The early dominance of resupinate morphologies was rapidly taken over by an array of more complex morphologies in the late Jurassic (~170–180 Myr), of which the pileate-stipitate type appears most dominant. This pattern could have been driven by the radiation of Agaricomycetidae, which contains the majority of pileate-stipitate species and started to diversify around this period, although pileate-stipitate species evolved in 12 orders as well, including the Russulales, Cantharellales and Gloeophyllales, among others. In the meanwhile, resupinate lineages may have simply continued to diversify at their previous rate, but, because of the radiation of species with pileate-stipitate fruiting bodies their dominance was diminished at the scale of the entire class. Consistent with this view, gains of the pileate-stipitate morphology are estimated to be significantly more likely (7–50 times, log(Bayes factor), logBF = 47) than their loss, indicating a trend towards pileate-stipitate morphologies, as reported earlier[13]. In fact, the pileate-stipitate morphology evolved convergently in at least 33 clades, suggesting it represents a stable attractor in the morphospace. Nevertheless, the probability of the loss of pileate-stipitate morphology is significantly larger than zero (logBF = 157.2), reflecting evolutionary transformations of pileate-stipitate fruiting bodies happening in many groups (Fig. 3c and Supplementary Data 1 and 7). We tested the impact of fruiting body morphologies on diversification rate in a character-state-dependent speciation and extinction framework[38,39]. Clades with pileate-stipitate fruiting bodies have a significantly higher speciation rate ($P < 10^{-16}$, likelihood ratio test, LRT) than clades with other morphologies (Fig. 3d and Supplementary Data 7). This may be because the pileate-stipitate morphology provides support and protection for developing spores (for example, from precipitation) and enhances their dispersal efficiency by raising sporogenous tissue above ground-level; these advantages may explain how pileate-stipitate fruiting bodies can promote diversification and suggest they represent a key innovation for mushroom-forming fungi

Conclusions

This study represents a global analysis of the dynamic evolutionary history of mushroom-forming fungi. The diversity of Agaricomycetes might have been shaped by both class-wide diversification rate shifts and explosive clade-specific events. We identified a major class-wide radiation of Agaricomycetes in the Jurassic, which possibly followed a warming and humid climate in this period. The onset of this radiation coincided with the expansion of angiosperms and followed patterns of gymno- and later angiosperm expansion during the Mesozoic-Cenozoic radiation[40]. Our analyses provide evidence for several clade-specific adaptive radiations in the class, offering a possible explanation for why some genera contain a single species, while others contain thousands. Our data display strong signal for a mass extinction event coinciding with increased extinction rates at the Jurassic/Cretaceous boundary, however, no such evidence was found in the Agaricomycetes for the much more influential Cretaceous–Tertiary mass extinction event. The evolution of pileate-stipitate fruiting bodies, that is, morphologies with cap and stipe might be a key driver of evolutionary radiations, suggesting that the convergent evolution of the classic mushroom morphology contributed to shaping extant diversity in the Agaricomycetes. We predict that further data on traits and ecological opportunities that generated the spectacular diversity of mushroom-forming fungi will help to elucidate the general principles of mushroom evolution and integrate this ecologically important group into the record of major biodiversification events.

Methods

Molecular biology methods. Genomic DNA was extracted from 0.1–10 mg of dried herbarium specimens using the DNeasy Plant Mini kit (Qiagen) or the Nucleospin Plant II mini kit (Macherey-Nagel) following the manufacturers' instructions. PCR amplification was performed as described previously[6,15] on the LSU of the nuclear ribosomal RNA with the LR7 and LROR primers. Sequencing was performed commercially using the same primers as used for PCR. Sanger reads were assembled to a contig using the Pregap and Gap4 programs of the Staden package[43] and checked manually against the electropherograms.

Taxon sampling. We sampled herbarium specimens so that taxon sampling be proportional across clades and geographic regions. To that end, we initially obtained estimates of the known diversity for each of the genera from Species Fungorum[44] (http://www.speciesfungorum.org), the Dictionary of the Fungi[16] and Funga Nordica[45]. Taxonomic information from these sources was compiled for all genera of Agaricomycetes. Using this compilation, we calculated the number of target species that needed to be sampled for each genus to obtain a final dataset of ~5,000 species (~30% sampling of total diversity) in which sampling of species in each genus is proportional to their described diversity. Although the three sources differed in their completeness, geographic scope (Dictionary of the Fungi and Species Fungorum being global databases and Funga Nordica being, taxonomically, the most stringent of the three) and taxonomic concept, it gave us general guidance on how to keep taxon sampling proportional across genera. When sampling species within genera, attempts have been made to obtain specimens from undersampled geographic regions—in particular, Africa, Asia, Australasia and South America.

Sequence alignment. Multiple sequence alignment was carried out for the LSU, ef-1a and RPB2 loci separately using the Probabilistic Alignment Kit (PRANK release 140603)[46,47]. An iterative alignment refinement strategy as described in Tóth et al.[48] was employed: maximum-likelihood gene trees computed from preliminary alignments (using RAxML, see below) were used as guide trees for the next round of multiple alignment for PRANK. After three rounds of iterative refinement, the alignments were further corrected manually using a text editor. Manual curation was restricted to correcting homologous regions erroneously juxtaposed by PRANK. Alignments of individual sequences were concatenated into a superalignment. The concatenated alignment is available at Dryad (accession number doi:10.5061/dryad.gc2k9r), GenBank accession numbers for all sequences used are shown in Supplementary Data 1.

Genome and transcriptome sequencing and assembly. *Sequencing.* The genomes of *Coprinopsis marcescibilis*, *Crucibulum laeve*, *Dendrothele bispora*, *Heliocybe sulcata*, *Peniophora* sp., *Pluteus cervinus*, *Polyporus arcularius* and *Pterula gracilis* were sequenced using a combination of fragment and long-mate pair Illumina libraries. In addition, the genome of *Coprinellus micaceus* was sequenced using Pacific Biosciences platform. Fragment Illumina genomic libraries were produced for 100 ng of DNA was sheared to 270 bp using the Covaris LE220 and size selected using SPRI beads (Beckman Coulter). The fragments were treated with end repair, A-tailing and ligation of Illumina compatible adaptors (IDT, Inc.) using the KAPA-Illumina library creation kit (KAPA biosystems). For long-mate pair libraries (*C. laeve*, *D. bispora*, *H. sulcata*, *P. arcularius* and *P. gracilis*), 5 µg of DNA was sheared using the Covaris g-TUBE and gel size selected for 4 kb. The sheared DNA was treated with end repair and ligated with biotinylated adaptors containing loxP. The adaptor ligated DNA fragments were circularized via recombination by a Cre excision reaction (NEB). The circularized DNA templates were then randomly sheared using the Covaris LE220 (Covaris). The sheared fragments were treated with end repair and A-tailing using the KAPA-Illumina library creation kit (KAPA Biosystems) followed by immobilization of mate pair fragments on strepavidin beads (Invitrogen). Illumina compatible adaptors (IDT, Inc.) were ligated to the mate pair fragments and eight cycles—or in the case of *Heliocybe sulcata* ten cycles—of PCR were used to enrich for the final library (KAPA Biosystems). For *C. micaceus* unamplified libraries were generated using the Pacific Biosciences standard template preparation protocol. Then, 5 µg of genomic DNA was used to generate each library and the DNA was sheared using Covaris g-Tubes to generate sheared fragments of 10 kb in length. The sheared DNA fragments were then prepared using the Pacific Biosciences SMRTbell template preparation kit, where the fragments were treated with DNA damage repair, had their ends repaired so that they were blunt-ended and 5' phosphorylated. Pacific Biosciences hairpin adaptors were then ligated to the fragments to create the SMRTbell template for sequencing. The SMRTbell templates were then purified using exonuclease treatments and size selected using AMPure PB beads.

All transcriptomes in this study were sequenced using Illumina RNA-Seq. Stranded complementary DNA libraries were generated using the Illumina Truseq Stranded RNA LT kit. Messenger RNA was purified from 1 µg of total RNA using magnetic beads containing poly-T oligos. mRNA was fragmented and reversed transcribed using random hexamers and SSII (Invitrogen) followed by second strand synthesis. The fragmented complementary DNA was treated with end-pair, A-tailing, adaptor ligation and ten cycles or, in the case of *C. marcescibilis*, *C. laeve* and *P. cervinus,* eight cycles of PCR.

The prepared Illumina libraries were quantified using KAPA Biosystem's next-generation sequencing library quantitative PCR kit and run on a Roche LightCycler 480 real-time PCR instrument. The quantified libraries were then multiplexed with other libraries, and the pool of libraries was then prepared for

sequencing on the Illumina HiSeq sequencing platform using a TruSeq paired-end cluster kit, v.4 and Illumina's cBot instrument to generate a clustered flow cell for sequencing. Sequencing of the flow cell was performed on the Illumina HiSeq2500 sequencer using HiSeq TruSeq SBS sequencing kits, v.4, following a 2×150 indexed run recipe. In the case of *C. micaceus*, *Dendrothele bispora*, *Peniophora* sp. and *P. arcularius*, TruSeq paired-end cluster kit, v.3, and TruSeq SBS sequencing kits, v.3, were used and in the cases of *C. laeve*, *H. sulcata* and *P. gracilis* a 2×100 indexed run recipe was performed.

For PacBio sequencing primer was annealed to the SMRTbell templates and Version P5 sequencing polymerase was bound to them. The prepared SMRTbell template libraries were then sequenced on a Pacific Biosciences RSII sequencer using Version C3 chemistry and 1×240 min sequencing movie run times.

Assembly and annotation. Genomic reads from each pair of Illumina libraries were QC filtered for artefact/process contamination and assembled together with AllPathsLG v.R49403[49]. Illumina reads of stranded RNA-seq data were used as input for de novo assembly of RNA contigs and assembled into consensus sequences using Rnnotator (v.3.4)[50]. The Pacific Biosciences sequence data were filtered with smrtanalysis assembled together with Falcon version 2014082 (ref. [51]), improved with finisherSC[52] and polished with Quiver. All genomes were annotated using the JGI Annotation Pipeline and made available via the JGI fungal portal MycoCosm[53]. Genome assemblies and annotation were also deposited at DDBJ/EMBL/GenBank.

Phylogenomic analysis of 104 Agaricomycotina. *Phylogenomic analysis.* The genome sequences of 104 species (Supplementary Table 1) were included in the phylogenomic analysis of Agaricomycotina. Two representatives of Tremellomycetes (*Tremella mesenterica* (Treme1), *Cryptococcus neoformans* var. *grubii* H99 (Cryne_H99_1)) were used as outgroups.

We performed all-versus-all blast using mpiBLAST 1.6.0 (ref. [54]) with default parameters, then identified gene families using the Markov clustering algorithm MCL 14-137 (ref. [55]) with an inflation parameter of 2.0. We first identified gene families that contained 52–208 genes (50–200% of the species included in the study), then performed multiple sequence alignment using PRANK 140603(ref. [47]). Ambiguously aligned regions were removed from the alignments using Gblocks 091b[56] with the settings -p=yes -b2=26 -b3=10 -b4=5 -b5=h -t=p -e=.gbl. Next, we screened for gene families that contained a single representative gene for each species, or ones that contained inparalogs but no deep paralogs. Deep paralogs were identified following Nagy et al.[57]. Gene trees were inferred using the PTHREADS version of RAxML 8.1.2 (ref. [58]) using the PROTGAMMAWAG model and the standard algorithm. A single inparalog, closest to the root on the basis of root-to-tip patristic distances was retained for each species. Gene families in which 75% or more of the species were represented were concatenated into a supermatrix.

We used RAxML 8.1.2 to perform maximum-likelihood analysis and bootstrapping on the concatenated dataset, under a WAG model with gamma-distributed rate heterogeneity partitioned by gene. We ran 100 bootstrap replicates using the rapid hill-climbing algorithm. Because in initial analyses *Peniophora* sp., *Tubaria furfuracea* and *Clavaria fumosa* were placed on long terminal branches, we performed the following steps to clean the alignments of overly divergent sequences (either due to sequencing errors or pseudogenes). We screened all individual gene trees and excluded proteins with a terminal branch length >2.75 times longer than the average branch length of the gene tree. Altogether, 1,294 (in 542 gene families) protein sequences were excluded from the analyses.

Sensitivity analysis. The robustness of the dataset was tested by eliminating incrementally higher numbers of fast-evolving sites using six levels of stringency in Gblocks 091b[56]. Using these parameters, we eliminated 8.5% (-b1=78 -b2=78 -b3=10 -b4=10), 24.3% (-b1=78 -b2=78 -b3=8 -b4=15), 36.7% (-b1=88 -b2=88 -b3=8 -b4=15), 46.4% (-b1=95 -b2=95 -b3=8 -b4=15), 50.1% (-b1=100 -b2=100 -b3=8 -b4=15) and 55.2% (-b2=104 -b3=5 -b4=20) of the least reliably aligned regions of the alignments, resulting in trimmed concatenated datasets with 129,886, 107,496, 89,732, 76,153, 70,862 and 63,309 amino acid sites, respectively. We performed maximum-likelihood phylogenetic inference for each of the reduced datasets in RAxML as described above.

Maximum likelihood analyses of the 5,284-taxon dataset. Maximum-likelihood trees for the 5,284-taxon dataset were inferred using the parallel version of RAxML v.8.1.2 (ref. [58]) under the generalized time-reversible model with gamma-distributed rate heterogeneity (four categories) with three partitions corresponding to the LSU, *ef1-α* and *rpb2* loci. The phylogenomic tree was used as a backbone monophyly constraint. We performed 245 maximum-likelihood inferences and tested whether these trees adequately represented the plausible set of topologies given the alignment. This was done to ensure that phylogenetic uncertainty is properly taken into account in subsequent comparative analyses. If our tree set contains all plausible topologies, then the rolling average of pairwise Robinson–Foulds distances should show a saturation as a function of increasing the number of trees. To this end, we computed Robinson–Foulds distance for each pair of trees for incrementally larger numbers of trees using R package 'phangorn' v.2.0.2 (ref. [59]). We then plotted the rolling average, maximum and minimum values as a function of the number of trees in R.

Molecular clock dating of the 5,284-taxon dataset. Due to computational limitations, we focused on ten maximum-likelihood trees that maximize topological diversity (as inferred on the basis of Robinson–Foulds distances) as representative trees for molecular clock analysis. These were chosen by first calculating pairwise Robinson–Foulds distances between trees, then hierarchically clustering trees using Ward's clustering method (as implemented in the hclust R function). The ten maximum-likelihood trees for subsequent analyses were chosen evenly from the resulting clusters of trees. To overcome the computational limitations of inferring accurate chronograms for thousand-tip phylogenies, we adopted a two-step strategy. First, PhyloBayes 4.1b[60] was used to infer parameters of a birth-death model and divergence times of trees on 10% subsampled versions of the 5,284-taxon dataset. Subsampled datasets were obtained by randomly deleting 90% of the species, but forcing key descendants of fossil-calibrated nodes to be retained in the subsampled alignments. Then we used the ages and parameters estimated in PhyloBayes as input parameters for FastDate development version[61] (provided by T. Flouri) for analysing the complete 5,284-species dataset.

PhyloBayes analyses were run using the 10% subsampled dataset, a birth-death prior on divergence times, an uncorrelated gamma multiplier relaxed clock model and a CAT-poisson substitution model with a gamma distribution on the rate across sites. A uniformly distributed prior was applied to fossil calibration times. All analyses were run until convergence, typically 15,000 cycles. Convergence of chains was assessed by visually inspecting the likelihood values of the trees and the tree height parameter. We sampled every tree from the posterior and after discarding the first 7,000 samples as burn-in we summarized the posterior estimates using the *readdiv* function of PhyloBayes.

Next, we used FastDate, a program that implements the speed dating algorithm described in Akerborg et al.[61]. FastDate was run on the complete trees (5,284 species) with the node ages constrained to the values of the 95% highest posterior densities of the ages inferred by PhyloBayes. FastDate analyses were run with time discretized into 1,000 intervals and the ratio of sampled extant individuals set to 0.14.

Fossil calibrations. The extensive sampling density of our tree allowed us to use more fossil calibration points than any study before and to place them more precisely within the tree. Eight fossils were used as calibration points (Supplementary Table 2) for the crown node of the specified taxa.

We excluded a number of prospective well-preserved fossils for reasons of redundantly calibrating an already calibrated node (*Appianoporites vancouverensis*—Hymenochaetales[62], *Protomycena electra*—marasmioid clade[63], *Cyathus dominicanus*—Nidulariaceae[64], *Fomes idahoensis*—Polyporales[65]. *Geastrum tepexensis*[66] was not considered as it could be assigned to either of the two earth-star clades, one in the Phallomycetidae (Geastraceae) or the other in the Boletales (*Astraeus*). For other mushroom fossils, the taxonomic affiliations were deemed too uncertain.

To investigate if there is any conflict between the fossil calibration points we conducted a fossil cross-validation analysis following Near et al.[67]. For this, we ran PhyloBayes analyses on one of the 10% subsampled trees with the same settings as mentioned above, using a single fossil calibration point at a time. This resulted in eight independent molecular dating analyses. To quantify conflict between single fossil calibrations, first we calculated the sum of the square differences between molecular age estimates and fossil ages:

$$SS_x = \sum_{i \neq x} D_i^2$$

where x is the fossil calibration point used and D_i is the difference between molecular age estimate and fossil age for fossil i. We ordered the SS values of each of the eight analyses in descending order and calculated the average squared deviation for all fossil calibrations:

$$s = \frac{\sum_{x=1}^{n} \sum_{i \neq x} D_i^2}{n(n-1)}$$

Next, the analysis with the highest SS value was removed and s was recalculated. We continued this process until only two analyses remained. In parallel, we performed one-tailed F-tests to check whether the removal of the fossil had a significant effect on the variance of s. The principle of this procedure is that during the stepwise removal of fossils, s should decrease by small constant values and variance should not decrease significantly

Genome-based molecular clock analyses. We examined the robustness of our molecular age estimates using phylogenomic methods as an alternative to the 5,284 species phylogeny. Specifically, we tested whether the differences between our and previous[17,18] molecular clock estimates for Agaricomycete orders were attributable to differences in the dataset or analytical method used or a difference in how precisely fossils could be placed on the tree. To this end, we performed a series of molecular clock analyses on our phylogenomic dataset that resembled that of Kohler and Floudas in terms of topology and taxon sampling density, but differed in the placement of some fossil calibrations. A key difference was that our phylogenomic tree included the most recent common ancestor (MRCA) of the Hymenochaetales and that of the Suillaceae, which allowed us to calibrate the MRCA of these clades,

as opposed to their stem nodes by Kohler et al.[18] and Floudas et al.[17] Further, our analysis includes the MRCA of the Nidulariaceae, a relatively recent node that can be calibrated by two well-preserved fossils described recently[64]

Phylogenomic dataset. We used a smaller, more conserved subset of the 568-gene and 104-species phylogenomic dataset (which was computationally not tractable in these analyses). First, we selected the first 70 most conserved genes of the 568-gene dataset by calculating the mean genetic distances for each gene using the dist.alignment function of the seqinR R package v.3.4-5 (ref. [68]). To enable a more accurate placement of fossil calibration points we added additional three species (*Cyathus striatus*, *Pycnoporus cinnabarinus*, *Suillus brevipes*) to this dataset (Supplementary Table 1) and excluded two taxa that harboured ambiguous positions. We searched homologous sequences in the additional genomes using blastp v.2.7.1 (ref. [69]) with one randomly selected gene from each of the 70 gene families as query. We selected the best hit (smallest *E*-value) as a one-to-one ortholog if the second best hit had a significantly worse *E*-value (by 20 orders of magnitude). Protein clusters were aligned by PRANK v.100802 (refs. [46,47]) using default settings. Next, conserved blocks of the alignments were selected using Gblocks v.0.91b[56] with default settings except for the minimum length of a block that was set to 5 and gap positions in half of the sequences were allowed. A phylogenomic tree was constructed by RAxML v.8.2.11 (ref. [58]) under the WAG + G substitution model partitioned by gene.

Calibrations. To dissect sources of differences in molecular age estimates, we ran analyses under three fossil calibration schemes (Supplementary Data 2) and the 105-species phylogenomic tree. First, we used the same fossil calibration scheme as for the 5,284-species phylogenetic dataset ('Default calibration scheme'). Next, we replicated the analyses of Kohler et al.[18] on our tree, using the fossil calibration points from Kohler et al. ('Kohler et al. calibration scheme 1'). For this, we placed the suilloid ectomycorrhiza fossil in the split of Suillinae/Paxillinae/Sclerodermatinae and *Archaeomarasmius leggettii* in the MRCA of *Gymnopus luxurians* and *Schizophyllum commune* with uniformly distributed 40–60 Myr and 70–110 Myr ago time priors, respectively. Finally, we used the calibrations used by Kohler et al. (scheme 2) but placed the two fossils in the MRCAs of the Suillaceae and marasmioid clade, respectively (Kohler et al.[18] calibration scheme 2'). In all analyses we constrained the age of the root to be between 300 Myr and 600 Myr ago.

Penalized likelihood analysis in r8s. We ran a series of molecular clock analyses in r8s v.1.81 (ref. [70]). A cross-validation analysis was performed to determine the optimal smoothing parameter (λ) by testing values across seven orders of magnitude starting from 10^{-3}. The additive penalty function was applied and the optimization was run 25 times starting from independent starting points. In one optimization step, after reaching an initial solution, the solution was perturbed and the truncated Newton optimization was rerun 20 times. We compared the results of previous studies to that of analyses across seven ancestral nodes in Agaricomycotina (Supplementary Data 2).

Bayesian molecular clock dating. We used the mcmctree method implemented in PAML v.4.8a[71]. The independent-rates clock model, a WAG substitution model and approximate likelihood calculation[72] were used. The birth rate, the death rate and the sampling fraction of the birth-death process were set to 1, 1 and 0.14, respectively. The shape and the concentration parameter of the gamma-Dirichlet prior for the drift rate coefficient (σ^2) was set to 1 and three different scale parameters were tested (10, 100, 1,000) to see their effect on the time estimates. The substitution rates of each gene were estimated by codeml under a global clock model, to set the parameters of the gamma-Dirichlet prior for the overall rate. By calculating the mean substitution rate of the loci and examining the density plot of the rates we set up a prior that reasonably fitted the data: the shape parameter, the scale parameter and the concentration parameter were set to 5, 90.7441 and 1, respectively, resulting in an average substitution rate per site per time unit of 0.055. We set the time unit to 100 Myr and applied uniform priors on eight fossil calibrations with lower and upper hard bounds. MCMC analysis was run for 80,000 iterations, discarding the first 20,000 iterations as a burn-in and sampling every 30th tree from the posterior. After three independent analyses were run the convergence of log-likelihood values was visually inspected and the estimated ages were compared between replicates.

Analyses of diversification and character evolution. *Character coding.* We discretely coded three characters, the presence of a cap, fruiting body type and substrate preference for the 5,284 species. Fruiting body types were coded as one of six types and data were compiled from the literature. The six character states distinguished were: (0) no fruiting body; (1) resupinate; (2) agaricoid; (3) cyphelloid; (4) gasteroid/secotioid and (5) coralloid/clavarioid. Transitional morphologies, or species for which no clear decision could be made on fruiting body type were coded as uncertain. Resupinate fruiting bodies were defined as crust-like or effused, flat morphologies that follow the morphology of the substrate, but irrespective of thickness or hymenophore type. The agaricoid type was defined as having a distinguishable stipe and cap. Cyphelloid species were coded following Bodensteiner[73]. The gasteroid types included species with closed fruiting bodies that produce spores internally. No distinction was made between secotioid, sequestrate and false-truffle morphologies and all were coded as gasteroid. Fruiting bodies with club-shaped or branched, erect morphology but no differentiated cap were considered coralloid/clavarioid.

The presence of a cap, that is pileate-stipitate morphology, was coded on the basis of literature data as either absent (state 0) or present (state 1). Species with rudimentary or reduced caps were coded as uncertain.

We coded species' preference for substrate on the basis of literature data (a detailed listing of resources used is not given) as gymnosperm, angiosperm or both (that is, generalist species). Species were considered gymno- or angiosperm specialists if >90% of records were for either plant group, or their habitat preferences in taxonomic literature were described by the terms 'exclusively', 'predominantly', 'mostly' or occurring on the least dominant substrate 'rarely', 'very rarely' or 'exceptionally'. On the other hand, species having records on both gymno- and angiosperm substrates, described in the literature as generalists or given multiple gymno- or angiosperm substrate plant species were coded as generalists. Species with insufficient data or no data at all were treated as missing data. Soil-inhabiting saprotrophs were coded on the basis of their association with either gymno- or angiosperms, if a clear preference was reported in the literature.

Tests of the LDG hypothesis. Global positioning system (GPS) data. We downloaded 5,884,445 fungal GPS records from the GBIF database, representing 4,429 Agaricomycetidae species. For 848 species, a location based on the province, country and/or biogeographic realm[74] was obtained from the literature. In cases where only the province, country or biogeographic realm was available, we took the centroid of the area as a proxy for GPS location. All GPS data were handled and processed in R[75]. Noise was added to identical GPS coordinates using the *jitter* function in R.

Analyses of geographic diversification. State-dependent diversification rates were estimated in two ways: (1) using centroid latitudes as continuous traits (for example, Sánchez-Ramírez et al.[35]) and (2) using discrete areas. We used the data mentioned above to first calculate a centroid coordinate (RGEOS R package) in cases where multiple GPS records exist per species. Then we took the centroid latitude for each species. For singletons, we simply took the latitude of each record. We also used the GPS database to calculate a standard deviation for latitude per species. For species with a single record, we took the mean standard deviation of species with multiple records. We fitted multiple Quantitative State Speciation and Extinction (QuaSSE[76]) models, using a maximum-likelihood approach, to ten of the 5,284-species chronograms. Models included speciation rate changes as a constant function of the trait (no effect), as a linear function or as a Gaussian function, keeping the extinction rate constant[76]. We also added two models in which the extinction rate varied as linear or Gaussian functions, while speciation rate remained constant. To improve the efficiency of the algorithm given the scale of the tree, we applied the following settings to the models: method = 'fftC', dt.max = 1 and nx = 256. Akaike information criterion values were averaged across phylogenies and compared between different models. We used the best supported model to interpolate speciation rates into a 1 × 1 degree global map made with Natural Earth. (Free vector and raster map data are available at www.naturalearthdata.com.)

To obtain discrete areas, first we divided all terrestrial WWF ecoregions into either tropical or extra-tropical. For tropical areas we considered: Tropical and Subtropical Moist Broadleaf Forests, Tropical and Subtropical Dry Broadleaf Forests, Tropical and Subtropical Grasslands, Savannas and Shrublands. All other terrestrial ecoregions were deemed extra-tropical. Ecoregion polygons were integrated (that is, dissolved) in a way that only two-state areas were found (Supplementary Note 7). For species with multiple GPS records, we extracted binary information about their presence in both areas. For records that were not found precisely within the geometry of the area, we took the area to which the distance to the GPS point was closer. To assign discrete states to each species with multiple records, our criterion was to assign a 'widespread' state (both areas) if records for the area with the minor frequency was higher than 0.2. In any other case, we assigned 'tropical' or 'extra-tropical' states to taxa in the area with the highest frequency. For taxa that had only biogeographic realm data, we coded them as follows: 'widespread': Neotropical, Afrotropical, Oceanian/Australia; 'tropical': Panamenian, Oriental and extra-tropical': Europe/Palaearctic/North Asia, Nearctic, Saharo-Arabian, Sino-Japanese. Using these three states for each taxon, we fitted multiple constrained models and one full model of Geographic State Speciation and Extinction (GeoSSE[77]) in a maximum-likelihood framework. The full model consisted of seven parameters: (1) speciation rate in the tropics, (2) speciation rate in the extra-tropical zone, (3) the allopatric speciation rate (speciation rate in both tropical and extra-tropical regions), (4) extinction rate in the tropics, (5) extinction rate in the extra-tropical zone, and dispersal rates to (6) the tropics and to (7) the extra-tropical zone. The constrained models consisted of: (1) speciation in the tropics is equal to speciation in the extra-tropical zone; (2) extinction in the tropics is equal to extinction in the extra-tropical zone and (3) dispersal to the tropics occurs at the same rate as dispersal to the extra-tropical zone. In each case, a single parameter for speciation, extinction, and dispersal was respectively estimated, allowing the other parameters of the model to vary. To explore the parameter space

better, we re-estimated parameters using MCMC on the full model. In a similar way as above, we used Akaike information criterion scores to rank the models.

Analyses of character evolution. Model tests. To infer substitution models that best describe the evolution of agaricoid/non-agaricoid fruiting bodies we used maximum-likelihood and MCMC approaches implemented in BayesTraits 2.0 Linux 64 Quad Precision alternative build[78] and the R package diversitree v.0.9–8 (ref. [39]). The BiSSE model[38] was used in diversitree. We performed model tests by first constraining the forward and reverse transition rates between non-agaricoid (state 0) and agaricoid type (state 1) to be equal ($q_{01}=q_{10}$). We also separately constrained each of the rates to be zero ($q_{01}=0$ or $q_{10}=0$). Each of the constrained models were compared to the best fit model on the basis of log-likelihood values (maximum-likelihood analyses in BayesTraits), log-Bayes factors (MCMC analyses in BayesTraits) or LRT and Akaike information criterion scores (maximum-likelihood analyses of BiSSE model in diversitree)[38,39,78,79]. In BayesTraits, a difference of 2.00 log-likelihood units (maximum-likelihood approach) or a difference of 10 log marginal likelihood units (MCMC approach) was considered as significant support for a model over another, while in the BiSSE analyses significance was assessed using LRTs ($P<0.05$).

BayesTraits analysis. BayesTraits analyses (maximum likelihood and MCMC) were performed on 245 phylogenetic trees using the MultiState module of the program. Before the final MCMC analyses, we tried several prior distributions (uniform, exponential, gamma and the hyper-prior versions of these) with different settings. On the basis of preliminary analyses, we found that the gamma distribution was most optimal, therefore in further analyses we used a gamma hyper-prior with different prior distributions for each parameter (Supplementary Note 5). All preliminary BayesTraits analyses were conducted with the following settings: 1,010,000 generations, 10,000 generations as burn-in and sampling every 500th generation. We forced Markov chains to spend 200,000 generations on each tree using the *equaltree* option, with 100,000 generations as burn-in and sampling every 500th generation. The marginal likelihood was estimated by the stepping stone method[78,80] using 50 stones with a chain length of 5,000. All analyses in BayesTraits were repeated three times to check the congruence of independent runs.

Diversitree analysis. We used ten chronograms to analyse trait-dependent diversification under the BiSSE model implemented in the R package diversitree v.0.9–10 (refs. [38,39]). Maximum-likelihood search started from the point in the parameter space determined by the function *starting.point.bisse*. Bayesian MCMC was performed using an exponential prior, defined as $1/(2r)$, where r is the character independent diversification rate. State-specific sampling fractions were defined on the basis of data from Species Fungorum[44] (see Accounting for random and incomplete taxon sampling). We first optimized the MCMC sampler's step size argument by running 100 generations, then we ran MCMC analyses for 20,000 generations with burn-in set to 10%. The convergence of the chains was visually checked on the basis of likelihood and parameter values.

Ancestral character-state reconstruction. We reconstructed the ancestral states using stochastic character mapping as implemented in *phytools* v.06–20 (ref. [81]), to reveal the dynamics of fruiting body types and substrate preference through time. This method is a modified version of a previously published algorithm[82], which samples discrete character histories from the posterior probability distribution. We performed the analysis with the *make.simmap* function on ten time-calibrated trees under a Markov model with all rates different. The stochastic character histories were simulated 5,000 times. We plotted state posterior probabilities through time using a custom R script. Briefly, we summarized character-state posterior probabilities through the time scale of our ten chronograms split into 100 bins. The plot was created using *ggplot* and *geom_area* functions of ggplot2 v.2.2.1 (ref. [83]). Ancestral probability distributions of substrate preference for the MRCAs of each of the orders and some additional clades were plotted as pie charts using the *nodelabels* function of *ape* v.4.1 (ref. [84]).

Diversification rate analyses. Accounting for random and incomplete taxon sampling. To meet the assumption of random or complete sampling of the BAMM and BiSSE models[20,39], we specified the sampling fraction of each genus in accordance with the described number of species based on Species Fungorum[44]. To gather information on described species, we screened all orders of the Agaricomycetes, Dacrymycetes and Tremellomycetes in Species Fungorum and gathered all species with a custom java program (available from the authors on request). We took into account taxonomic and nomenclatural synonymy if indicated by Species Fungorum. We accounted for incomplete taxon sampling by two strategies. First, we assigned specific sampling fractions to the character states (BiSSE model) or to genera (BAMM model). In these cases we used the built-in correction of the BiSSE and BAMM models[20,85] to account for missing species in our phylogeny. Second, because we could have unintentionally oversampled certain genera (for example, because of better availability of specimens), we statistically tested for oversampling and generated a pruned phylogeny in which each genus is represented in proportion of its described diversity. We adjusted taxon sampling in our phylogeny by iteratively deleting species from genera that were oversampled relative to the mean sampling fraction of the tree, until sampling fractions of each genera corresponded their known size as judged by a comparison to Species Fungorum. To do this, we performed a hypergeometric test ($P<0.05$) at each iteration of species removal. Elimination of species was stopped when oversampling disappeared ($P>0.05$, hypergeometric test). With this procedure we wanted to produce a 'skeletal tree' (sensu FitzJohn et al.[85]), where species were both evenly and randomly sampled from every genera[85].

Trait-dependent diversification rate analyses. We performed analyses under the BiSSE model to examine the effect of agaricoid fruiting body type on diversification rate. BiSSE analyses were carried out in diversitree v.09–10 as described above, with the following differences. We performed model tests to examine if the presence of a cap influenced speciation and extinction rates. To this end, we first constrained state-specific speciation or extinction rates to be equal ($\lambda_0=\lambda_1$ or $\mu_0=\mu_1$) then constrained both the speciation rates and extinction rates to be equal ($\lambda_0=\lambda_1$ and $\mu_0=\mu_1$). Models were compared by LRT in R.

Trait-independent diversification rate analyses. We used BAMM v.2.5.0 (ref. [20]) to examine rate heterogeneity across lineages and detect shifts in diversification rates. We analysed ten chronograms and ran MCMC analyses for 100 million generations using four independent chains per analysis with 50 million generations as burn-in. Prior parameters were optimized using the *setBAMMpriors* function in BAMMtools v.2.1.6 (ref. [86]), except for the prior on the expected number of shifts, which was set to 270 on the basis of preliminary runs. We accounted for incomplete taxon sampling as described above. We checked the convergence of chains by visually inspecting the convergence of likelihoods, by calculating the effective sample size and the Geweke's diagnostic[87] of log-likelihoods, numbers of shifts and evolutionary rate parameters, using functions in CODA 0.19-1 (ref. [88]). Geweke's diagnostic tests for the quasi equality of the means of parameters sampled at different parts of the MCMC analysis; it means that, if the beginning and end regions of the post-burn-in MCMC sample do not differ to a statistically significant extent ($P>0.05$), then the Markov chain is considered to be in a stationary phase. To ensure that a shift is highly supported by the data and the prior had negligible contribution, we examined only core shifts; that is, those with a prior-to-posterior marginal odds ratio exceeding 5 (ref. [86]86

We compared core shifts across ten chronograms to obtain a consensus view on shifts that can be detected in all or most of the trees. To this end, we first empirically identified taxonomically similar clades for which a core shift was inferred, taking into account topological differences among trees. Then we noted whether the mean diversification rate change after the shift is positive or negative (that is, rate acceleration or deceleration). There were cases when several core shifts were inferred on adjacent branches around the MRCA of a given clade. These come from distinct shift configurations sampled during the MCMC analysis and correspond to the same signal of rate variation in the data but were located to adjacent branches of the tree. In such cases, we chose the shift with the highest posterior probability, noting that the biological reality of increasing rates might be spread out across a few adjacent branches around the one with the highest posterior. Finally, shifts were referred to as congruent core shifts if they were highly congruent across four or more trees and had strong tree support (mean posterior probability >0.5).

Next, we assessed whether posterior probabilities of congruent core shifts reached convergence in a fashion similar to the 'cumulative' function of AWTY[89]. For this, we calculated the posterior probability of each core shift at each generation, as if the analysis was stopped at that point and plotted posterior probabilities as a function of generation using the ggplot2 v.2.2.1 package[83]. We also took into account the distinct shift configurations by examining whether a rate increase, after a congruent core shift was explained by a rate decrease after another core shift. First, we determined congruent core shift—core shift pairs that could potentially be mutually exclusive to each other. These shift pairs were determined in one tree, usually in the tree where a congruent core shift had high posterior probability. Then we calculated two kinds of posterior proportions: one for co-occurring shift pairs and one for each of the single occurrence of the shifts. We said that two shifts were mutually exclusive to each other if only a negligible co-occurrence was presented and the direction of the diversification rate change was different between the single occurrence posterior samples.

To reveal tree-wide evolutionary patterns we calculated average net rates through time using the *getRateThroughTimeMatrix* function and plotted by the *plotRateThroughTime* function of the BAMM package.

Validation of BAMM estimates. There have been critics of the BAMM method recently[90,91]. Meyer and Wiens[91] found that the method-of-moments estimator yielded stronger relationship between true and estimated diversification rates than BAMM, particularly in smaller clades. Therefore, to validate the BAMM results we used the method-of-moments estimator on clades with congruent core shifts. The method-of-moments approach estimates diversification rates from species richness and clade age while it can incorporate incomplete taxon sampling and extinction rate by assuming a relative extinction fraction (ε = extinction rate / speciation rate)[92]. We used the *bd.ms* function in *geiger 2.0.6* (ref. [93]). The analyses were performed on all the 85 clades with congruent core shifts, using three different

relative extinction fractions (0, 0.45, 9) and calculating with both stem and crown ages. We calculated unsampled species fractions using the genus-specific sampling fractions we determined for BAMM analyses. For the same set of clades we calculated average net diversification and net speciation rates from BAMM data using the *getCladeRates* function. Then we performed linear regressions between method-of-moments estimates with different settings and average net diversification or net speciation rates from BAMM. We examined the adjusted r^2 and the *P* values of the models to evaluate the correspondence between the two methods.

Detecting mass extinction events. We performed analyses using the compound Poisson process on mass extinction times model (CoMET)[27,94], to examine tree-wide variation in diversification rate and occurrence of mass extinctions during the evolution of mushroom-forming fungi. First, we conducted a model comparison on ten chronograms using the CoMET model with a constant rate birth-death process implemented in the TESS 2.1.0. R package[95]. We compared models with and without mass extinction events on the basis of marginal likelihoods. We allowed the occurrence of a mass extinction event along the entire time span of a tree and we set the survival probability of species to 0.1 (corresponding to 10% of the species surviving a mass extinction event). The overall sampling fraction of species was set to 0.14. MCMC analyses were run for 20,000 generations and the first 2,000 posterior samples were discarded as a burn-in. Marginal likelihoods were estimated using stepping stone simulation using 100 stepping stones.

Then, we performed reversible jump Markov chain Monte Carlo (rjMCMC) analyses under the CoMET model to sample from the space of episodically varying birth-death processes with mass extinction events. In this analysis, we also tested the significance of the occurrence of a mass extinction event by performing model tests within time intervals. Bayes factor values $BF > 10$ or $\ln BF > 6$ were considered strong support for a model, following Höhna et al.[96] and Kass and Raftery[97]. We examined the sensitivity of the posterior probabilities to different prior settings in preliminary analyses of a randomly chosen tree. We examined models with two or ten expected mass extinction events, with 30, 100 or 270 expected rate changes and with survival probabilities of 0.001, 0.05 or 0.3. All of these preliminary analyses were run for 1.6 million generations with 100,000 generations as burn-in. We used a log-normal prior on speciation and extinction rates with a mean of 0.2 and 0.15 and a standard deviation of 0.5 and 0.5, respectively. In the final analyses we used all ten chronograms and an empirical hyper-prior on rate parameters on the basis of 200,000 iterations with 100,000 burn-in. The priors on the number of expected mass extinction and the expected rate changes were set to 2 and 30, respectively, on the basis of results of preliminary analyses. We set the survival probability to 0.05. Analyses were run for 3 million generations with 1 million generations as burn-in. The convergence of the analyses was checked by visually inspecting the log-likelihood values and by computing the effective sample size and the Geweke diagnostic for the log-likelihoods, the number of speciation rate shifts, the number of extinction rate shifts and the number of mass extinction events using the *effectiveSize* and the *geweke.diag* function of the *CODA* 0.19.-1 package[88], respectively. To check the convergence of interval-specific parameters we used the *tess.plot.singlechain.diagnostics* function of the *TESS* package.

Reporting Summary. Further information on research design is available in the Nature Research Reporting Summary linked to this article.

Data availability

New sequence data generated for this study were deposited at DDBJ/EMBL/GenBank under the accession numbers MK277471–MK278670 and MK299400–MK299412. Trees and alignments have been deposited in Dryad Digital Repository (accession number: doi:10.5061/dryad.gc2k9r). Genome assembly and annotation of *C. micaceus FP101781*, *C. marcescibilis CBS121175*, *C. laeve CBS166.37*, *Dendrothele bispora CBS962.96*, *H. sulcata OMC1185*, *Peniophora* sp. *Cont*, *P. cervinus NL-1719*, *P. arcularius HBB13444* and *P. gracilis CBS309.79* were deposited at DDBJ/EMBL/GenBank under the accession numbers QPFP00000000, QPFQ00000000, QPFR00000000, QPKH00000000, QPFL00000000, LOAU00000000, QPFM00000000, QPFN00000000 and QPFO00000000. All custom code is available from the authors upon request.

Received: 9 August 2018; Accepted: 30 January 2019;

References

1. Jetz, W. & Pyron, R. A. The interplay of past diversification and evolutionary isolation with present imperilment across the amphibian tree of life. *Nat. Ecol. Evol.* **2**, 850–858 (2018).
2. Jetz, W., Thomas, G. H., Joy, J. B., Hartmann, K. & Mooers, A. O. The global diversity of birds in space and time. *Nature* **491**, 444–448 (2012).
3. Rabosky, D. L. et al. Rates of speciation and morphological evolution are correlated across the largest vertebrate radiation. *Nat. Commun.* **4**, 1958 (2013).
4. Alfaro, M. E. et al. Explosive diversification of marine fishes at the Cretaceous–Palaeogene boundary. *Nat. Ecol. Evol.* **2**, 688–696 (2018).
5. Alfaro, M. E. et al. Nine exceptional radiations plus high turnover explain species diversity in jawed vertebrates. *Proc. Natl Acad. Sci. USA* **106**, 13410–13414 (2009).
6. Nagy, L. G. et al. The evolution of defense mechanisms correlate with the explosive diversification of autodigesting coprinellus mushrooms (Agaricales, fungi). *Syst. Biol.* **61**, 595–607 (2012).
7. Wilson, A. W., Hosaka, K. & Mueller, G. M. Evolution of ectomycorrhizas as a driver of diversification and biogeographic patterns in the model mycorrhizal mushroom genus Laccaria. *New Phytol.* **213**, 1862–1873 (2017).
8. Wilson, A. W., Binder, M. & Hibbett, D. S. Diversity and evolution of ectomycorrhizal host associations in the sclerodermatineae (Boletales, Basidiomycota). *New Phytol.* **194**, 1079–1095 (2012).
9. Sánchez-Ramírez, S., Tulloss, R. E., Amalfi, M. & Moncalvo, J. M. Palaeotropical origins, boreotropical distribution and increased rates of diversification in a clade of edible ectomycorrhizal mushrooms (Amanita section Caesareae). *J. Biogeogr.* **42**, 351–363 (2015).
10. Sánchez-Garcia, M. & Matheny, P. B. Is the switch to an ectomycorrhizal state an evolutionary key innovation in mushroom-forming fungi? A case study in the Tricholomatineae (Agaricales). *Evolution* **71**, 51–65 (2017).
11. Wilson, A. W., Binder, M. & Hibbett, D. S. Effects of gasteroid fruiting body morphology on diversification rates in three independent clades of fungi estimated using binary state speciation and extinction analysis. *Evolution* **65**, 1305–1322 (2011).
12. Hibbett, D. S. After the gold rush, or before the flood? Evolutionary morphology of mushroom-forming fungi (Agaricomycetes) in the early 21st century. *Mycol. Res.* **111**, 1001–1018 (2007).
13. Hibbett, D. S. Trends in morphological evolution in homobasidiomycetes inferred using maximum likelihood: a comparison of binary and multistate approaches. *Syst. Biol.* **53**, 889–903 (2004).
14. Hibbett, D. S. & Binder, M. Evolution of complex fruiting-body morphologies in homobasidiomycetes. *Proc. Biol. Sci.* **269**, 1963–1969 (2002).
15. Matheny, P. B. et al. Major clades of Agaricales: a multilocus phylogenetic overview. *Mycologia* **98**, 982–995 (2006).
16. Kirk, P, Cannon, P. & Minter, D. *Dictionary of the Fungi* (CABI International, Wallingford, UK, 2011).
17. Floudas, D. et al. The Paleozoic origin of enzymatic lignin decomposition reconstructed from 31 fungal genomes. *Science* **336**, 1715–1719 (2012).
18. Kohler, A. et al. Convergent losses of decay mechanisms and rapid turnover of symbiosis genes in mycorrhizal mutualists. *Nat. Genet.* **47**, 410–415 (2015).
19. Lutzoni, F. et al. Contemporaneous radiations of fungi and plants linked to symbiosis. *Nat. Commun.* **9**, 5451 (2018).
20. Rabosky, D. L. Automatic detection of key innovations, rate shifts, and diversity-dependence on phylogenetic trees. *PLoS ONE* **9**, e89543 (2014).
21. McKenna, D. D., Sequeira, A. S., Marvaldi, A. E. & Farrell, B. D. Temporal lags and overlap in the diversification of weevils and flowering plants. *Proc. Natl Acad. Sci. USA* **106**, 7083–7088 (2009).
22. Looney, B. P., Ryberg, M., Hampe, F., Sánchez-García, M. & Matheny, P. B. Into and out of the tropics: global diversification patterns in a hyperdiverse clade of ectomycorrhizal fungi. *Mol. Ecol.* **25**, 630–647 (2016).
23. Krah, F.-S. et al. Evolutionary dynamics of host specialization in wood-decay fungi. *BMC Evol. Biol.* **18**, 119 (2018).
24. Beaulieu, J. M. & O'Meara, B. C. Extinction can be estimated from moderately sized molecular phylogenies. *Evolution* **69**, 1036–1043 (2015).
25. Rabosky, D. L. Challenges in the estimation of extinction from molecular phylogenies: a response to Beaulieu and O'Meara. *Evolution* **70**, 218–228 (2016).
26. Rabosky, D. L. Extinction rates should not be estimated from molecular phylogenies. *Evolution* **64**, 1816–1824 (2010).
27. May, M. R., Hohna, S. & Moore, B. R. A Bayesian approach for detecting the impact of mass-extinction events on molecular phylogenies when rates of lineage diversification may vary. *Methods Ecol. Evol.* **7**, 947–959 (2016).
28. Tennant, J. P., Mannion, P. D., Upchurch, P., Sutton, M. D. & Price, G. D. Biotic and environmental dynamics through the late jurassic-early cretaceous transition: evidence for protracted faunal and ecological turnover. *Biol. Rev.* **92**, 776–814 (2017).
29. Casadevall, A. Fungi and the rise of mammals. *PLoS Pathog.* **8**, e1002808 (2012).
30. Vajda, V. & McLoughlin, S. Fungal proliferation at the Cretaceous–Tertiary boundary. *Science* **303**, 1489–1489 (2004).
31. Mittelbach, G. G. et al. Evolution and the latitudinal diversity gradient: speciation, extinction and biogeography. *Ecology Lett.* **10**, 315–331 (2007).
32. Peay, K. G., Kennedy, P. G. & Talbot, J. M. Dimensions of biodiversity in the Earth mycobiome. *Nat. Rev. Microbiol.* **14**, 434–447 (2016).
33. Shi, L.-L. et al. Variation in forest soil fungal diversity along a latitudinal gradient. *Fungal Divers.* **64**, 305–315 (2014).
34. Tedersoo, L. et al. Global diversity and geography of soil fungi. *Science* **346**, 1256688–1256688 (2014).

35. Sánchez-Ramírez, S., Etienne, R. S. & Moncalvo, J. M. High speciation rate at temperate latitudes explains unusual diversity gradients in a clade of Ectomycorrhizal fungi. *Evolution* **69**, 2196–2209 (2015).
36. Gavrilets, S. & Losos, J. B. Adaptive radiation: contrasting theory with data. *Science* **323**, 732–737 (2009).
37. Givnish, T. J. Adaptive radiation versus 'radiation' and 'explosive diversification': why conceptual distinctions are fundamental to understanding evolution. *New Phytol.* **207**, 297–303 (2015).
38. Maddison, W. P., Midford, P. E. & Otto, S. P. Estimating a binary character's effect on speciation and extinction. *Syst. Biol.* **56**, 701–710 (2007).
39. Fitzjohn, R. G. Diversitree: Comparative phylogenetic analyses of diversification in R. *Methods Ecol. Evol.* **3**, 1084–1092 (2012).
40. Berendse, F. & Scheffer, M. The angiosperm radiation revisited, an ecological explanation for Darwin's 'abominable mystery'. *Ecol. Lett* **12**, 865–872 (2009).
41. Niklas, K. J., Tiffney, B. H. & Knoll, A. H. Patterns in vascular land plant diversification. *Nature* **303**, 614–616 (1983).
42. Berner, R. A. Phanerozoic atmospheric oxygen: new results using the GEOCARBSULF model. *Am. J. Sci.* **309**, 603–606 (2009).
43. Staden, R. The Staden sequence analysis package. *Mol. Biotechnol.* **5**, 233–241 (1996).
44. *Species Fungorum* (CABI/Royal Botanic Gardens Kew, 2018).
45. Knudsen, H. & Vesterholt, J. *Funga Nordica: Agaricoid, Boletoid and Cyphelloid Genera* (Nordsvamp:Copenhagen, 2008).
46. Loytynoja, A. & Goldman, N. Phylogeny-aware gap placement prevents errors in sequence alignment and evolutionary analysis. *Science* **320**, 1632–1635 (2008).
47. Loytynoja, A. & Goldman, N. From The Cover: an algorithm for progressive multiple alignment of sequences with insertions. *Proc. Natl Acad. Sci. USA* **102**, 10557–10562 (2005).
48. Tóth, A. et al. Iteratively refined guide trees help improving alignment and phylogenetic inference in the mushroom family bolbitiaceae. *PLoS ONE* **8**, e56143 (2013).
49. Gnerre, S. et al. High-quality draft assemblies of mammalian genomes from massively parallel sequence data. *Proc. Natl Acad. Sci. USA* **108**, 1513–1518 (2011).
50. Martin, J. et al. Rnnotator: an automated de novo transcriptome assembly pipeline from stranded RNA-Seq reads. *BMC Genomics* **11**, 663 (2010).
51. Chin, C.-S. et al. Phased diploid genome assembly with single-molecule real-time sequencing. *Nat. Methods* **13**, 1050–1054 (2016).
52. Lam, K.-K., LaButti, K., Khalak, A. & Tse, D. FinisherSC: a repeat-aware tool for upgrading de novo assembly using long reads. *Bioinformatics* **31**, 3207–3209 (2015).
53. Grigoriev, I. V. et al. MycoCosm portal: gearing up for 1000 fungal genomes. *Nucleic Acids Res.* 42(699), 704–(2014).
54. Darling, A., Carey, L. & Feng, W. The design, implementation, and evaluation of mpiBLAST. in *ClusterWorld Conference & Expo and the 4th International Conference on Linux Clusters: The HPC Revolution 2003. LA-UR 03-2862* (2003).
55. van Dongen, S. *Graph Clustering by Flow Simulation*. PhD thesis, Univ. Utrecht (2000).
56. Talavera, G. & Castresana, J. Improvement of phylogenies after removing divergent and ambiguously aligned blocks from protein sequence alignments. *Syst. Biol.* **56**, 564–577 (2007).
57. Nagy, L. G. et al. Comparative genomics of early-diverging mushroom-forming fungi provides insights into the origins of lignocellulose decay capabilities. *Mol. Biol. Evol.* **33**, 959–970 (2016).
58. Stamatakis, A. RAxML version 8: a tool for phylogenetic analysis and post-analysis of large phylogenies. *Bioinformatics* **30**, 1312–1313 (2014).
59. Schliep, K. P. phangorn: phylogenetic analysis in R. *Bioinformatics* **27**, 592–593 (2011).
60. Lartillot, N., Lepage, T. & Blanquart, S. PhyloBayes 3: a Bayesian software package for phylogenetic reconstruction and molecular dating. *Bioinformatics* **25**, 2286–2288 (2009).
61. Åkerborg, Ö., Sennblad, B. & Lagergren, J. Birth-death prior on phylogeny and speed dating. *BMC Evol. Biol.* 8, 77 (2008).
62. Smith, S. Y., Currah, R. S. & Stockey, R. A. Cretaceous and eocene poroid hymenophores from Vancouver Island, British Columbia. *Mycologia* **96**, 180–186 (2004).
63. Hibbett, D. S., Grimaldi, D. & Donoghue, M. J. Fossil mushrooms from Miocene and Cretaceous ambers and the evolution of homobasidiomycetes. *Am. J. Bot.* **84**, 981–991 (1997).
64. Poinar, G. Bird's nest fungi (Nidulariales: Nidulariaceae) in Baltic and Dominican amber. *Fungal Biol* **118**, 325–329 (2014).
65. BrownR. W A bracket fungus from the late Tertiary of southwestern Idaho. *J. Washington Acad. Sci.* **30**, 422–424 (1940).
66. Magallon-Puebla, S. & Cevallos-Ferriz, S. R. S. A fossil earthstar (Geasteraceae; Gasteromycetes) from the late cenozoic of puebla, mexico. *Am. J. Bot.* **80**, 1162–1167 (1993).
67. Near, T. J., Meylan, P. A. & Shaffer, H. B. Assessing concordance of fossil calibration points in molecular clock studies: an example using turtles. *Am. Nat.* **165**, 137–146 (2005).
68. Charif, D. & Lobry, J. R. *SeqinR 1.0-2: A Contributed Package to the R Project for Statistical Computing Devoted to Biological Sequences Retrieval and Analysis* (Springer, Berlin, 2007); https://doi.org/10.1007/978-3-540-35306-5_10
69. Camacho, C. et al. BLAST+: architecture and applications. *BMC Bioinformatics* **10**, 1–9 (2009).
70. Sanderson, M. J. Estimating absolute rates of molecular evolution and divergence times: a penalized likelihood approach. *Mol. Biol. Evol.* **19**, 101–109 (2002).
71. Yang, Z. PAML 4: phylogenetic analysis by maximum likelihood. *Mol. Biol. Evol.* **24**, 1586–1591 (2007).
72. Thorne, J. L., Kishino, H. & Painter, I. S. Estimating the rate of evolution of the rate of molecular evolution. *Mol. Biol. Evol.* **15**, 1647–1657 (1998).
73. Bodensteiner, P., Binder, M., Moncalvo, J. M., Agerer, R. & S Hibbett, D. Phylogenetic relationships of cyphelloid homobasidiomycetes. *Mol. Phylogenet. Evol.* **33**, 501–515 (2004).
74. Holt, B. G. et al. An update of Wallace's zoogeographic regions of the world. *Science* **339**, 74–78 (2013).
75. R: A Language and Environment for Statistical Computing (R Core Team, 2018).
76. Fitzjohn, R. G. Quantitative traits and diversification. *Syst. Biol.* **59**, 619–633 (2010).
77. Goldberg, E. E., Lancaster, L. T. & Ree, R. H. Phylogenetic inference of reciprocal effects between geographic range evolution and diversification. *Syst. Biol.* **60**, 451–465 (2011).
78. Pagel, M. & Meade, A. BayesTraits v.3.0.1 (Reading Evolutionary Biology Group, 2007).
79. Pagel, M. Inferring the historical patterns of biological evolution. *Nature* **401**, 877–884 (1999).
80. Xie, W., Lewis, P. O., Fan, Y., Kuo, L. & Chen, M. H. Improving marginal likelihood estimation for bayesian phylogenetic model selection. *Syst. Biol.* **60**, 150–160 (2011).
81. Revell, L. J. phytools: an R package for phylogenetic comparative biology (and other things). *Methods Ecol. Evol.* **3**, 217–223 (2012).
82. Huelsenbeck, J. P., Nielsen, R. & Bollback, J. P. Stochastic mapping of morphological characters. *Syst. Biol.* **52**, 131–158 (2003).
83. Wickham, H. *Ggplot2. Elegant Graphics for Data Analysis* (Springer, New York, 2009); https://doi.org/10.1007/978-0-387-98141-3
84. Paradis, E., Claude, J. & Strimmer, K. APE: Analyses of phylogenetics and evolution in R language. *Bioinformatics* **20**, 289–290 (2004).
85. Fitzjohn, R. G., Maddison, W. P. & Otto, S. P. Estimating trait-dependent speciation and extinction rates from incompletely resolved phylogenies. *Syst. Biol.* **58**, 595–611 (2009).
86. Rabosky, D. L. et al. BAMMtools: an R package for the analysis of evolutionary dynamics on phylogenetic trees. *Methods Ecol. Evol.* **5**, 701–707 (2014).
87. Geweke, J. Evaluating the accuracy of sampling-based approaches to the calculation of posterior moments. *Bayesian Stat.* **4**, 169–193 (1992).
88. Plummer, M., Best, N., Cowles, K. & Vines, K. CODA: convergence diagnosis and output analysis for MCMC. *R News* **6**, 7–11 (2006).
89. Nylander, J. A. A., Wilgenbusch, J. C., Warren, D. L. & Swofford, D. L. AWTY (are we there yet?): a system for graphical exploration of MCMC convergence in Bayesian phylogenetics. *Bioinformatics* **24**, 581–583 (2008).
90. Moore, B. R., Höhna, S., May, M. R., Rannala, B. & Huelsenbeck, J. P. Critically evaluating the theory and performance of Bayesian analysis of macroevolutionary mixtures. *Proc. Natl Acad. Sci. USA* **113**, 9569–9574 (2016).
91. MeyerA. L. S. & WiensJ. J. Estimating diversification rates for higher taxa: BAMM can give problematic estimate of rates and rate shifts. *Evolution* **72**, 1–15 (2017).
92. Magallon, S. & Sanderson, M. J. Absolute diversification rates in angiosperms clades. *Evolution* **55**, 1762–1780 (2001).
93. Harmon, L. J., Weir, J. T., Brock, C. D., Glor, R. E. & Challenger, W. GEIGER: investigating evolutionary radiations. *Bioinformatics* **24**, 129–131 (2008).
94. Höhna, S. The time-dependent reconstructed evolutionary process with a key-role for mass-extinction events. *J. Theor. Biol.* **380**, 321–331 (2015).
95. Höhna, S. Fast simulation of reconstructed phylogenies under global time-dependent birth-death processes. *Bioinformatics* **29**, 1367–1374 (2013).
96. Hohna, S., May, M. R. & Moore, B. R. *Phylogeny Simulation and Diversification Rate Analysis with TESS*; https://cran.r-project.org/web/packages/TESS/vignettes/Bayesian_Diversification_Rate_Analysis.pdf 1–98 (2015).
97. Kass, R. E. & Raftery, A. E. Bayes factors. *J. Am. Stat. Assoc.* **90**, 773–795 (1995).

Acknowledgements

We want to thank I. Nagy for help in writing a custom java program to retrieve species from the Species Fungorum database. This work has received funding from the Momentum Program of the Hungarian Academy of Sciences (contract no. LP2014/12, to L.G.N.) and from the European Research Council (ERC) under

the European Union's Horizon 2020 research and innovation programme (grant agreement no. 758161). The work by the U.S. Department of Energy Joint Genome Institute, a DOE Office of Science User Facility, is supported by the Office of Science of the U.S. Department of Energy under contract no. DE-AC02-05CH11231. T.V. was supported by the National Talent Program (contract no. NTP-NFTÖ-17-B-0337), by the UNKP-18-3 New National Excellence Program of the Ministry of Human Capacities and by the Straub Young Scientist scholarship from the Biological Research Centre, Hungarian Academy of Sciences. The support of V.A. was provided to the Moravian Museum by the Ministry of Culture of the Czech Republic (DKRVO, ref. MK000094862).

Author contributions

B.D., J.G.S., B.K., J.U., S.K. and V.B. sequenced specimens, W.A, K.W.B., M.C., S.H., K.L.B., A.L., S.M., R.R., F.M.M. and I.V.G. sequenced, assembled, and annotated genomes. K.K., T.V. J.G.S. and L.G.N made multiple alignment, K.K. performed phylogenomic analyses. G.S. and T.V. conducted molecular dating. A.F.J., A.S., A.S., B.B., B.D., B.E.L., B.O.S., C.A., C.F., C.O., C.S., C.V., D.D., D.K., H.K., I.K., J.C., J.G., K.H., K.L., K.S., L.A., L.M., M.E.N., M.T., N.L.B., N.R., O.M., P.B., P.C., P.F., R.E.T., S.K., S.S.R., T.N., T.P., V.A., V.S., W.D. and Z.L. contributed specimens or sequences. K.K., T.V., B.D., V.P., V.B., C.F. and O.M. worked on character coding of species. S.S.R. tested the LDG hypothesis. M.S.G. performed BiSSE analyes. C.F. and T.V. conducted BayesTraits analyses. All other analyses were performed by T.V. L.G.N., K.K., T.V., M.S.G., S.S.R. and D.S.H. wrote the article. L.G.N. supervised the project. All authors read and commented on the manuscript.

Competing interests

The authors declare no competing interests.

Additional information

Supplementary information is available for this paper at https://doi.org/10.1038/s41559-019-0834-1.

Reprints and permissions information is available at www.nature.com/reprints.

Correspondence and requests for materials should be addressed to L.G.N.

Publisher's note: Springer Nature remains neutral with regard to jurisdictional claims in published maps and institutional affiliations.

[1]Synthetic and Systems Biology Unit, Biological Research Centre, Hungarian Academy of Sciences, Szeged, Hungary. [2]Department of Plant Anatomy, Institute of Biology, Eötvös Loránd University, Budapest, Hungary. [3]Clark University, Worcester, MA, USA. [4]Department of Ecology and Evolutionary Biology, University of Toronto, Toronto, Ontario, Canada. [5]MTA-ELTE 'Lendület' Evolutionary Genomics Research Group, Department of Biological Physics, Eötvös Loránd University, Budapest, Hungary. [6]Department of Microbiology, Faculty of Science and Informatics, University of Szeged, Szeged, Hungary. [7]Department of Botany, Faculty of Horticultural Science, Szent István University, Budapest, Hungary. [8]Hungarian Mycological Society, Budapest, Hungary. [9]US Department of Energy Joint Genome Institute, Walnut Creek, CA, USA. [10]Via Cappuccini 78, Pordenone, Italy. [11]Jardin Botanico Nacional Ma. Moscoso, Santo Domingo, Dominican Republic. [12]Department of Botany, Moravian Museum, Brno, Czech Republic. [13]Science and Conservation, Department of Biodiversity, Western Australian Herbarium, Kensington, WA, Australia. [14]Manaaki Whenua—Landcare Research, Auckland, New Zealand. [15]Institut de Systématique, Evolution, Biodiversité (ISYEB—UMR 7205), Muséum National d'Histoire Naturelle, Sorbonne Université, CNRS, Paris, France. [16]State Herbarium of South Australia, Adelaide, South Australia, Australia. [17]Manaaki Whenua—Landcare Research, Lincoln, New Zealand. [18]Oberfeldstraße 9, St. Georgen bei Salzburg, Austria. [19]Department of Biology, San Francisco State University, San Francisco, CA, USA. [20]Zsombolyai u. 56., Székesfehérvár, Hungary. [21]Naturalis Biodiversity Center, Leiden, the Netherlands. [22]Department of Ecology and Evolutionary Biology, University of Tennessee, Knoxville, TN, USA. [23]Department of Mycology, W. Szafer Institute of Botany, Polish Academy of Sciences, Kraków, Poland. [24]Natural History Museum, Slovak National Museum, Bratislava, Slovakia. [25]Biodiversity Unit, Finnish Environment Institute, Helsinki, Finland. [26]Instituto de Micología y Botánica, CONICET—Universidad de Buenos Aires, Buenos Aires, Argentina. [27]The Jodrell Laboratory, Royal Botanic Gardens, Kew, UK. [28]Damjanich u. 54, Budapest, Hungary. [29]Department of Biology, Microbiology, Utrecht University, Utrecht, the Netherlands. [30]Center for Forest Mycology Research, Northern Research Station, US Forest Service, Madison, WI, USA. [31]Department of Biology, University of Central Oklahoma, Edmond, OK, USA. [32]Botanical Museum, University of Helsinki, Helsinki, Finland. [33]Institute of Plant and Animal Ecology, Russian Academy of Sciences, Ekaterinburg, Russia. [34]Department of Cryptogamic Botany, Swedish Museum of Natural History, Stockholm, Sweden. [35]Faculty of Forestry and Wood Technology, Mendel University in Brno, Brno, Czech Republic. [36]Herbarium Rooseveltensis Amanitarum, Roosevelt, NJ, USA. [37]The New York Botanical Garden, New York, NY, USA. [38]Plant and Microbial Biology, University of California, Berkeley, CA, USA. [39]Department of Plant and Microbial Biology, University of California Berkeley, Berkeley, CA, USA. [40]Institut National de la Recherche Agronomique, Laboratory of Excellence Advanced Research on the Biology of Tree and Forest Ecosystems, Champenoux, France. [41]Present address: Section for Genetics and Evolutionary Biology, University of Oslo, Oslo, Norway. [42]Present address: Institute of Ecology and Earth Sciences, University of Tartu, Tartu, Estonia. [43]Present address: MTA-SZTE 'Lendulet' Fungal Pathogenicity Mechanisms Research Group, Szeged, Hungary. *e-mail: lnagy@fungenomelab.com

Supplementary Information for

Megaphylogeny resolves global patterns of mushroom evolution

Torda Varga, Krisztina Krizsán, Csenge Földi, Bálint Dima, Marisol Sánchez-García, Santiago Sánchez-Ramírez, Gergely J. Szöllősi, János G. Szarkándi, Viktor Papp, László Albert, William Andreopoulos, Claudio Angelini, Vladimír Antonín, Kerrie W. Barry, Neale L. Bougher, Peter Buchanan, Bart Buyck, Viktória Bense, Pam Catcheside, Mansi Chovatia, Jerry Cooper, Wolfgang Dämon, Dennis Desjardin, Péter Finy, József Geml, Sajeet Haridas, Karen Hughes, Alfredo F. Justo, Dariusz Karasiński, Ivona Kautmanova, Brigitta Kiss, Sándor Kocsubé, Heikki Kotiranta, Kurt M. LaButti, Bernardo E. Lechner, Kare Liimatainen, Anna Lipzen, Zoltán Lukács, Sirma Mihaltcheva, Louis Morgado, Tuula Niskanen, Machiel E. Noordeloos, Robin A. Ohm, Beatriz Ortiz-Santana, Clark Ovrebo, Nikolett Rácz, Robert Riley, Anton Savchenko, Anton Shiryaev, Karl Soop, Viacheslav Spirin, Csilla Szebenyi, Michal Tomšovský, Rodham E. Tulloss, Jessie Uehling, Igor V. Grigoriev, Csaba Vágvölgyi, Tamás Papp, Francis M. Martin, Otto Miettinen, David S. Hibbett, László G. Nagy

Published in Nature Ecology and Evolution.

This PDF file includes:

Supplementary Notes 1 to 8

Supplementary Figures 1 to 10

Supplementary Tables 1 to 8

Captions for Supplementary Data 1 to 7

Table of contents

Supplementary Note 1.: Phylogenomic analysis

Phylogenomics results - The phylogenomic analysis of Agaricomycotina included 104 genomes from 18 orders of the Agaricomycetes, as well as Dacrymycetes and Tremellomycetes (Supplementary Table 1.). We detected 663 gene families that contained a single gene per species or, if multiple genes per species were found they were inparalogs of each other. Of these, 650 contained genes from at least 75% of the species, which were concatenated into a supermatrix of 141.951 amino acid sites. Our analyses are in agreement with previous phylogenomic studies, but included members of Phallales, Gomphales and Thelephorales in phylogenomic studies for the first time.

Sensitivity analysis - Rapidly evolving sites can be a source of noise and may lead to incorrect topologies due to model violations; removal of these sites can improve phylogenetic signal[1]. To test the robustness of our results, ambiguously aligned amino acid sites were removed in an incremental manner. We discarded 8.5–55.2% of the sites of the original dataset in six steps, resulting in incrementally shorter and more conserved datasets, which, however, conferred minor changes in the inferred topologies and bootstrap values, which were limited to weakly supported branches. For example, the Pluteaceae proved to have an unstable position: in the original dataset it was placed as a weekly supported (BS 67%) sister group of Amanitaceae whereas it clustered together with the Tricholomatineae (sensu Dentinger et al.[2]) upon removal of 36.8% of the original dataset (BS 32%). Removal of 50.1% of the sites yielded a tree topology on which the Pluteaceae grouped together with the Macrocystidiaceae (BS 45%) (Supplementary Fig 2. C-F). Other changes observed upon the exclusion of 8.5–24.3 % of the original dataset were the repositioning of *Fibroporia radiculosa* as the earliest branching taxon of the antrodia clade. However, upon further exclusion of sites, this taxon returns to its original position as, the sister group of *Postia placenta* (BS 100%) on an unsupported branch (BS <50%) in the antrodia clade of Polyporales (Supplementary Fig 2. A, B). The exclusion of 24.3–36.8 % of the original dataset caused the reordering of groups in the Phallales-Geastrales-Gomphales-Trechisporales. It has also led to the relocation of *Sistotremastrum niveocremeum* (Supplementary Fig 2. B, C).

Phylogenomic relationships in the Agaricomycotina - Our trees confirmed previous results for most branches, although we inferred stronger support for certain groupings or contradicting relationships compared to previous genome-based or multigene studies. In the next section, we discuss nodes of the Agaricomycotina in detail that deviate from previous studies in placement. The Tremellomycetes, represented by two members of Tremellales (*Tremella mesenterica* and *Cryptococcus neoformans* var. *grubii*), were used as an outgroup. The Dacrymycetes formed a strongly supported sister group of Agaricomycetes in contrast with Zhao et al.[3], where this topology was not well-supported (BS 55%), but in agreement with the majority of other phylogenomic studies[4–6]. Our phylogeny supports the early divergence of the Cantharellales, Sebacinales and Auriculariales in the Agaricomycetes as it has been described previously[4–7]. The Phallomycetidae in our analysis showed sister group relationship with the Trechisporales (BS 85%, Supplementary Fig 1) in accordance previous studies[3], although some studies suggested that the Trechisporales forms an independent lineage branching prior to Hymenochaetales and the remaining Agaricomycetes[5,8,9]. The position of the clade formed by Gloeophyllales, Jaapiales, and Corticiales remained ambiguous previously[8]. Some studies suggested this clade to be a sister of the Polyporales[3,5] or of the Agaricomycetidae[10], while others suggested that this clade is the sister group to the clade formed by the Russulales and Agaricomycetidae[6,8,11]. Additionally, Binder et al.[12] inferred a clade comprising *Gloeophyllum*, corticioid, russuloid and polyporoid clades, but not the Jaapiales. This latter was placed as the

sister group of the euagarics, boletoid and athelioid clades. Our results showed partial congruence with these findings: the Gloeophyllales, Jaapiales and Corticiales formed a strongly supported clade sister to (BS 93%) the clade formed by Russulales, Theleophorales, and Polyporales. On a higher-level, these groups were sister to the Agaricomycetidae. In line with this, our phylogeny did not confirm the sister group relationship of Russulales and Agaricomycetidae[3,6–9]. We inferred the Russulales as the sister to the clade formed by the Polyporales, Gloeophyllales, Jaapiales and Corticiales (BS 93%). Within this clade the Russulales was the sister group of the Thelephorales and Polyporales (BS 56%) (Supplementary Fig. 1). The sister group relationship of the Polyporales and Thelephorales was mentioned by Hibbett[4] and Matheny[9] and was confirmed in these study with strong support (BS 100%). However, the Thelephorales was represented by only a single species (*Thelephora ganbajun*), as more sequenced genomes will be available, this relationship should be further tested.

The monophyly of Polyporales has been robustly demonstrated by several previous studies[7,11–13]; however, the composition and support of the subclades therein remained unresolved. Similarly to the 356- and 71-gene-based phylogeny of Binder et al.[11] the four major clades of the Polyporales (antrodia clade, gelatoporia clade, core polyporoid clade, phlebioid clade) and their branching order were confirmed with strong support (BS 100%) using an extended sampling of genomes in this study. Whereas our taxon set improved sampling in the gelatoporia, the antrodia, the core polyporoid and the phlebioid clades compared to Binder et al.[11], no new genomes were involved in the phylogenomic analysis from the more problematic "residual polyporoid" clade.

Our results did not resolve the two higher-level clades suggested by Justo et al.[13] based on nrITS, nrLSU and *rpb1*: one contained *Candelabrochaete africana*, the "phlebioid" and "residual polyporoid" clades, while the other included the "core polyporoid", "gelatoporia", "antrodia" and "skeletocutis-tyromyces" groups. Our dataset did not include species from the "residual polyporoid" and "*Tyromyces*" clades, however. Although the antrodia clade itself was well supported, within the clade we found poor support for the branching at *Fibroporia radiculosa* and *Postia placenta*, and for the grouping of this clade with that formed by *Wolfiporia cocos* and *Laetiporus sulphureus* var. *sulphureus*. For clarifying the branching order and relationship of these clades the inclusion of additional genomes will be necessary.

The topology of the major groups of Agaricomycetidae is in accordance with previous phylogenomic[5,6,8] and phylogenetic studies[9,10,14–17] that supported the sister group relationship of Amylocorticiales-Atheliales and Boletales, which together formed the sister group of the Agaricales. Within the Boletales, branches are well supported and are in full agreement with the results based on the phylogenetic relationships inferred from 5.8S rRNA, *rpb1*, *rpb2*, and *tef1* in the study of Binder et al.[10] and previous phylogenomic inferences[3,5,6].

Relationships in the Agaricales were largely congruent with that of Dentinger et al.[2]. Within the Agaricales we determined a highly supported (BS 100%) clade formed by *Schizophyllum commune* and *Fistulina hepatica* that corresponds to the Schizophyllineae[2], but this is in contrast with the recent study of Zhao et al.[3], which found the Shcizophyllaceae and Pterulaceae to group together, based on a six-gene phylogeny. On our tree, the Schizophyllaceae branched after the Hygrophorinae (consisting of the Clavariaceae and Hygrophoraceae) and Pleurotinae (including the Pleurotaceae and Pterulaceae) split off of the backbone, which is consistent with the tree of Dentinger et al.[2], but is in contrast with other previous studies[5,6] with sparser taxon sampling. Additionally, we resolved the weakly supported clade of Physalacriaceae, Cyphellaceae, and hydropoid clade, among which the Cyphellaceae and hydropoid clade are sister groups and branch before the Physalacriaceae (BS 97%). Furthermore, the Marasmiineae clade according to

Dentinger et. al.[2] was supplemented by *Dendrothele bisporus* in our dataset, which formed the strongly supported sister lineage (BS 100%) of Omphalotaceae.
The clade corresponding to Pluteineae[2] forms a sister group of the clade equivalent to Agaricineae[2] in our results (BS 63%), but this relationship received lower support than that found by Dentinger et al. (BS 80%). Besides, we found the same moderately supported sister relationship between the Amanitaceae and Pluteaceae (BS 67%) as Dentinger et al. (BS 69%), even though, the Pluteaceae was supplemented with *Pluteus cervinus* in our study. The Pluteaceae proved unstable in our sensitivity analysis as well: with the removal of increasing amounts of the fastest-evolving sites from original dataset the Pluteaceae either grouped together with the Tricholomataceae (BS 32%) or was paraphyletic (BS 61%), but no longer formed a monophyletic group together with the Amanitaceae. Future studies should include either more species of Pluteaceae or construct more informative datasets to help resolve this contentious part of the Agaricales phylogeny.
A well-supported clade corresponding to the Tricholomatineae (BS 100%)[2] could be resolved in our study. A strongly supported sister relationship of *Macrocystidia cucumis* and *Infundibulicybe gibba* (BS 100%) was inferred for first time here, which resolved the inconsistent placement of these taxa in the study of Dentinger et al.[2].
Recent phylogenomic[2,5,6] and phylogenetic[3] studies found the Psathyrellaceae to branch off before the Hydnangiaceae, except Matheny et al.[14], who proposed the sister group relationship of these two groups. Our results, involving additional two species of the Psathyrellaceae (*Coprinopsis marcescibilis*, *C. micaceus*), but only one species of Hydnangiaceae (*Laccaria bicolor*) confirm Matheny et al's results and supports the sister group relationship of Hydnangiaceae and Psathyrellaceae (BS 100%).

Supplementary Note 2.: Phylogenetic analyses of the 5,284 species dataset

Sequence alignment - Overall 5,284 species have been sampled from the Agaricomycetes, Dacrymycetes and Tremellomycetes from which the latter was used as an outgroup. Three loci, nrLSU (4,835 species) *rpb2* (1,252 species) and *ef1-α* (721 species) were included in the analyses. The final alignment contained 6,905 characters in total, from which we excluded 1,168 ambiguously aligned sites (including intronic regions) to obtain a final length of 5,737 characters. Of this, the length of individual partitions was 1,052 for *tef1-α*, 2,768 for nrLSU and 1,917 for *rpb2*.

Phylogenetic tree reconstruction: Maximum Likelihood analyses - Maximum likelihood (ML) trees for the 5,284-species dataset were inferred as it was described in the Materials and Methods. We performed 245 ML inferences and tested whether these trees adequately represented the plausible set of topologies given the alignment by examining the Robinson-Foulds (RF) distances across trees. Because the maximum, the average and the minimum of the RF values were saturated (Supplementary Fig. 3.) we stopped to generate trees after the 247th ML run.

Supplementary Note 3.: Newly sequenced genomes

To fill some gaps in the genome-scale phylogeny of the Agaricomycetes, we sequenced the genomes of nine species, listed in Supplementary Table 1. Sequencing was performed on either Illumina or PacBio platforms and resulted in 74x - 141x coverage and assembly sizes ranging from 32 Mb to 131 Mb. The largest assembly was obtained for *Dendrothele bispora*, a highly reduced corticioid species in the Agaricales. This species also had the highest number of predicted genes (33,645). In terms of fragmentation, *Heliocybe sulcata* had the least fragmented genome with 87 scaffolds, followed by *Pterula gracilis* and *Crucibulum laeve*. Uniformly, 40 - 62% of the predicted genes had InterPro-based annotations.

The rationale for selecting species was based on current sampling of Agaricomycetes orders and families within the Agaricales. Of the nine species, *Crucibulum laeve* is the first sequenced representative of the Nidulariaceae, an enigmatic family in the Agaricales containing 'bird's-nest fungi' with highly specialized morphologies and dispersal strategies. Similarly, *Pluteus cervinus* is a representative of the Pluteaceae, from which only *Volvariella volvacea* has been available previously. The *Pluteus* genome was sequenced from field-collected fruiting bodies and surprisingly contained <1% of bacterial contaminating sequence reads. *Pterula gracilis* is an early-diverging member of the Agaricales and the first sequenced species in the Pterulaceae. It shows affinities to pleurotoid and schizophylloid species and fills an important gap in the genomic sampling of the Agaricales. Outside the Agaricales, we sequenced *Peniophora* sp, which is an early-branching member of the Russulales (Peniophoraceae), whereas *Polyporus arcularius* and *Heliocybe sulcata* belong to the Polyporales and Gloeophyllales, respectively.

<u>*Assembly and annotation*</u> - Genomic reads from both libraries were QC filtered for artifact/process contamination and assembled together with AllPathsLG v. R49403[18]. Illumina reads of stranded RNA-seq data were used as input for de novo assembly of RNA contigs, assembled into consensus sequences using Rnnotator (v. 3.4)[19]. All genomes were annotated using the JGI Annotation Pipeline and made available via the JGI fungal portal MycoCosm[20]. Genome assemblies and annotation were also deposited at DDBJ/EMBL/GenBank (see main text for accession numbers).

Supplementary Note 4.: Molecular dating

Assessing fossil calibration signal - Both PhyloBayes and FastDate analyses reached convergence (data not shown). The fossil cross-validation analysis suggested that there is no conflict between fossil calibrations points (Supplementary Fig. 4.), so we used all fossils in subsequent analyses. By comparing the age estimates for clades with that from recent molecular clock studies[6,7] we found that our estimates were comparably older. For example the emergence of Agaricales was dated to 90 and 108 mya by Floudas et al.[7] and Kohler et al.[6], respectively while our mean estimated ages ranged between 160-182 mya depending on the tree analyzed (Supplementary Data 2). The differences could come from the different data set (the analyses of Floudas et al.[7] and Kohler et al.[6] based on genomes), taxon sampling density or the calibration schemes used in the analyses. To address the causes of the difference in age estimates, we performed molecular dating on genomic data under various calibration schemes.
The following fossils were considered as potential calibration points, but were excluded either because of uncertainties in their taxonomic placement or redundancy with other, more informative fossils for our dataset:

Fomes mattirolii - Age: Miocene (5.3–23 million years ago) Site: Libya. Taxonomic assignment uncertain and the fossil is too recent (Miocene) to inform calibration of the tree. Reference: Zuffardi-Comerci, R., 1934. Fomes (Polyporus) Mattirolii n. sp. nel Miocene della Libia. Missione Scientifica della Reale Accademia d'Italia a Cufra (1931-IX), vol. 3, pp. 58–60.

Archeterobasidium syrtae - Age: Miocene (5.3–23 million years ago) Site: Libya. Similar to *Ganodermites libycus*, belongs to Ganodermataceae, but too recent (Miocene) to be informative. Reference: Koeniguer, J.C., Locquin, M.V., 1979. Un polypore fossile à spores porées du Miocène de Libye: Archeterobasidium syrtae, gen. et sp. nov. In: Ministère des Universités Comité des Travaux Historiques et Scientifiques (Ed.), Comptes Rendus du 104e Congrès National des Sociétés Savantes, Bordeaux, 1979, fasc. I (Paléobotanique). Paris (France), Bibliothèque Nationale, pp. 323–329.

Fomites libyae - Age: Miocene (5.3-23 million years ago) Site: Libya. No photo available of the fossil, presumably similar to *Fomes*. Too recent (Miocene). Reference: Locquin, M.V., Koeniguer, J.C., 1981. Un nouveau polypore fossile du Miocène de Libye: Fomites libyae Locquin et Koeniger, gen. et sp. nov. In: Ministère des Universités comité des Travaux Historiques et Scientifiques (Ed.), Comptes Rendus du 106e Congrès National des Sociétés Savantes, Perpignan, 1981, fasc. I (Paléontologie). Paris (France), Bibliothèque Nationale, pp. 107–117.

***Polyporus* sp.** - Age: Miocene (5.3–23 million years ago) Site: Libya. No photo of the fossil found, publication could not be accessed. Reference: Mayr, H., 2006. Fossilien. BLV Buchverlag GmbH, Munich (Germany), 255 pp.

Ganoderma adspersum - Age: Miocene (5–23 million years ago) Site: Netherlands. Too recent. Reference: Fraaye, R.H.B., Fraaye, M.W., 1995. Miocene bracket fungi (Basidiomycetes, Aphyllophorales) from the Netherlands. Contrib. Tert. Quat. Geol. 32, 27–33.

Ganoderma applanatum - Age: Pleistocene (2.6–0.01 million years ago) Site: Alaska, USA. Too recent. Reference: Chaney, R.W., Mason, H.L., 1936. A Pleistocene flora from Fairbanks, Alaska. Amer. Mus. Nat. Hist. Novitates 877, 1–17.

Ganoderma lucidum - I.Age: Pleistocene (2.6–0.01 million years ago) Site: Alaska, USA. II.Age: Pleistocene (2.6–0.01 million years ago) and Holocene (0.01 ma–today). Too recent. References: Chaney, R.W., Mason, H.L., 1936. A Pleistocene flora from Fairbanks, Alaska. Amer. Mus. Nat. Hist. Novitates 877, 1–17. Kopczyński, K., 2006. Zapis kopalny grzybów i organizmów grzybopodobnych (Fossil record of fungi and pseudofungi). Prz. Geol. 54, 231–237 (in Polish with an English abstract).

Fomes idahoensis - Age: Pliocene (5.3–2.6 million years ago) Site: Idaho, USA, Too recent. Reference: Brown, R. W., (1940): A bracket fungus from the late Tertiary of southwestern Idaho. – Ibidem, 30: 422–424., Buchwald, N. F., (1970): Fomes idahoensis Brown. A fossil polypore fungus from the Late Tertiary of Idaho,U. S. A. – Friesia 9: 339–340.

Trametites ginkgoides - Age: Pliocene (5.3–2.6 million years ago) Site: Germany, Too recent. References: Straus, A., 1952a. Beiträge zur Pliozänflora von Willershausen III. Die niederen Pflanzengruppen bis zu den Gymnospermen. Palaeontogr., Abt. B 93, 1–44., Straus, A., 1952b. Pilze aus dem Pliozän von Willershausen (Kr. Osterode, Harz). Z. Pilzkd. 21, 11–14.

Appianoporites vancouverensis - Age: Eocene (56–34 million years ago) Site: Vancouver, Canada. Redundant with Quatsinoporites. Reference: Selena, Y. S., Randolph, S. C., Ruth, A. S., Cretaceous and Eocene poroid hymenophores from Vancouver Island, British Columbia Mycologia, 96(1), 2004, pp. 180–186.

Coprinites dominicanus - Age: Miocene (20–16 million years ago) Site: Dominican Republic, Taxonomic assignment uncertain, too recent to calibrate higher-level categories (e.g. Agaricales). Reference: George, O. P., Jr. and Rolf, S., Upper Eocene Gilled Mushroom from the Dominican Republic Science, New Series, Vol. 248, No. 4959 (Jun. 1, 1990), pp. 1099–1101.

Protomycena electra - Age: Miocene (25–15 million years ago) Site: Dominican Republic. Redundant with *Archaeomarasmius*, but more recent. Reference: Hibbett, D.S., Grimaldi, D.S., Donoghue, M.J., (1997). Fossil mushrooms from Miocene and Cretaceous Ambers and the evolution of Homobasidiomycetes American Journal of Botany 84 (8), 981–991.

Aureofungus yaniguaensis - Age: Miocene (25–15 million years ago) Site: Dominican Republic. Too recent, taxonomic position uncertain. Reference: Hibbett D., Binder M., Zheng, W., Yale, G., Another fossil agaric from Dominican amber Mycologia, 95(4), 2003, pp. 685–687.

Cyathus dominicanus - Age: Oligocene–Miocene (30–15 million years ago) Site: Dominican Republic. Redundant with *Nidula baltica* but more recent. Reference: Poinar, Jr. G., (2014). Bird's nest fungi (Nidulariales: Nidulariaceae) in Baltic and Dominican amber. Fungal Biology, 118(3), 325–329.

Bovista plumbea - Age: Pleistocene (2.6–0.01 million years ago) Site: Alaska, USA. Too recent. Reference: Chaney, R.W., Mason, H.L., 1936. A Pleistocene flora from Fairbanks, Alaska. Amer. Mus. Nat. Hist. Novitates 877, 1–17.

Lycoperdites tertiarius - Age: Oligocene–Miocene (26–22 million years ago) Site: Mexico Position as a true puffball (Lycoperdaceae) is uncertain. Reference: POINAR, G.O., JR.,

2001. Fossil Puffballs (Gasteromycetes: Lycoperdales) in Mexican amber. Historical Biol. 15,219–222.

Geastrum tepexensis - Age: Miocene–Pleistocene (8–5 million years ago) Site: Mexico. Taxonomically it could either belong to Geastrales or *Astraeus*. Reference: Magallon-Pueble, S. & R.S. Cervallos-Ferriz, 1993. A fossil earthstar (Geasteraceae; Gasteromycetes) from the Late Cenozoic of Pueblo, Mexico. Amer. J. Bot. 80, 1162–1167.

Geastroidea lobata - Age: Late Cretaceous (72-66 million years ago) Site: Mongolia. The characters of the fossil cannot be evaluated based on the photographs. Reference: Krassilov, V.A., Makulbekov, N.M., 2003. First find of Gasteromycetes (fungi) in the Cretaceous deposits of Mongolia. Paleontological Journal 37, 439–442.

Palaeogaster micromorphus - Age: Mid-Cretaceous (97–110 million years ago) Site: Myanmar (Burma). Taxonomic assignment uncertain. Reference: George, O. P., Jr., Dônis da Silva, A., Iuri, G. B., A Gasteroid fungus, Paleogaster micromorpha gen. & sp. nov. (Boletales) in Cretaceous Myanmar Amber. Journal of the Botanical Research Institute of Texas 8(1)), 139–143. 2014.

Palaeoclavaria burmitis - Age: Mid-Cretaceous (110–100 million years ago) Site: Myanmar (Burma) Taxonomic affinity as a clavarioid fungus is doubtful. Reference: Poinar, G.O., JR. & A.E. Brown., 2003. A non-gilled hymenomycete in Cretaceous amber. Mycological Res. 107: 763–768.

Molecular clock analysis of genome-scale data - The reduced dataset used for molecular clock dating contained 105 species, 70 genes and 18,917 amino acid characters. Cross-validation analyses in r8s yielded 10 or 100 as the best smoothing parameter for penalized likelihood analyses. In mcmctree, all MCMC chains converged to stationary distributions as judged from log-likelihood values and the three independent MCMC replicates yielded congruent age estimates. We found that models with a scale parameter of 1000 for the gamma-Dirichlet prior were >127 times more unlikely than models with a scale parameter 100 or 10, so we chose a scale parameter of 100 for subsequent analyses in mcmctree.

We first assessed the impact of the placement of calibration points on the tree. When we placed the fossils used by Kohler et al.[6] to the exact same positions on the tree as in the previous study, we obtained similar, but slightly older estimates for most nodes: 126 myr and 131 myr for the Agaricales and the Agaricomycetidae, compared to 108 myr and 125 myr by Kohler et al.[6], respectively ("Kohler et al. calibration scheme 1") (Supplementary Data 2). Assigning suilloid ectomycorrhizae and *Archaemarasmius* to the more precisely defined ancestors of the Suillaceae and of the marasmioid clade (due to new genome sequences available to us) yielded considerably older estimates, 169 myr and 176 myr for the Agaricales and the Agaricomycetidae, respectively ("Kohler et al. calibration scheme 2"). Adding another 6 fossils to the analysis ("Default calibration scheme") yielded 156 myr and 162 myr for these nodes, a comparably small change from the 2-fossil calibration scheme, suggesting that molecular age estimates are primarily driven by the precision of the placement of fossil calibrations on the tree and to a smaller extent by the set of fossil calibration points used (Supplementary Data 2).

The divergence times estimated by mcmctree were generally older than those estimated by r8s and were more similar to the ages inferred with the 5,284-species tree (Supplementary Fig. 5). The mean age of the Agaricomycetidae was estimated at 182 myr, 20 myr older than by r8s, but 3 myr younger than the mean across the 10 chronograms containing 5,284 species. The age of

the Agaricales and the Boletales were inferred at 175 and 166 myr, as opposed to 156 and 150 by r8s, respectively. Larger differences were obtained for more ancient nodes, which might be related to differences in how the root was constrained in the different analyses. The mrca of Agaricomycetes was inferred at 317 myr, 46 myr older than the date given by r8s. That of the Agaricomycetes and Dacrymycetes was inferred at 385 myr in mcmctree as opposed to 314 myr in r8s. Despite these differences, analyses in mcmctree and r8s are consistent in that they both suggest that the Agaricomycetidae and most orders therein originated in the Jurassic period.

Supplementary Note 5.: Trait evolution

Analyses of character evolution - Analyses of the evolution of agaricoid fruiting body type in BayesTraits showed that gains of the pileate-stipitate morphology were favored during evolution (Supplementary Data 7, Fig. 3/d). The average transition rates from the non-pileate towards the pileate-stipitate state (q_{01}) were 6.9–51.5 times higher than in the reverse direction (q_{10}) depending on the method (ML or MCMC). Constraining the rates of gain and loss to be equal ($q_{01} = q_{10}$) resulted in significantly lower likelihoods (40 log-likelihood units, logBF: 47), suggesting that models with equal gain and loss rates can be rejected. The biggest differences from the null model were found when the rate of gain of the pileate-stipitate morphology (q_{01}) was forced to be zero (383 log-likelihood units, log BF: 382). Models with the reverse rate (q_{10}, loss of pileate-stipitate type) constrained to zero were also significantly different from the null model (159 log-likelihood units, log BF: 157), which suggests that the transition from pileate-stipitate to non-pileate types was also important during the evolution of mushroom forming fungi. Analyses performed under the BiSSE model yielded similar results (Supplementary Data 7, Fig. 3/d). In BISSE, the average transition rates from the non-pileate towards the pileate-stipitate state (q_{01}) were 13.2–14.2 times higher than in the reverse direction (q_{10}). All the constrained BiSSE models ($q_{01} = q_{10}$ or $q_{01} = 0$ or $q_{01} = 0$) yielded significantly worse likelihoods than the null model according to likelihood ratio tests ($p < 0.001$, Supplementary Data 7).

Ancestral character state reconstruction - We found that the transition rate matrices estimated during the ancestral state reconstruction (ASR) analyses contained highly similar values across trees in case of both traits (fruiting body types and substrate/host preference) examined in this study (Supplementary Data 3). In case of fruiting body types, species with resupinate or no fruiting bodies dominated the first periods of the evolution of Agaricomycetes. Then, around 180 million years ago, complex fruiting body types (agaricoid, cyphelloid, gasteroid/secotioid, coralloid/clavarioid) appeared and the cumulative posterior probability of the agaricoid type started to increase until it became the dominant fruiting body type (see Fig. 3 in main text). In parallel, the prevalence of resupinate fruiting body types decreased. This essentially suggests that resupinate fruiting bodies were phased out by the agaricoid type as the most widespread fruiting body morphology. It should be noted, however, that this does not necessarily mean that resupinate lineages became less diverse or went extinct, rather, it means that the proliferation of agaricoid lineages leads to resupinate ones sharing a lower fraction of the cumulative posterior probability.

ASR of species' preference for substrate (either gymnosperm or angiosperm) revealed that the Boletales, Polyporales, Russulales, Hymenochaetales and Phallomycetidae, all dated close to or in the Jurassic period, likely had ancestors with a gymnosperm preference (posterior probability, PP > 0.70). The MRCA of the Agaricales had an unresolved substrate preference (PP of gymnosperm substrate: 0.54). Of the orders dated to the Jurassic, only the MRCA of the Sebacinales and that of the Cantharellales showed higher probabilities for angiosperm than gymnosperm substrates (PP = 0.91 and 0.87, respectively). Smaller orders that emerged after the Jurassic were associated with either gymno- or angiosperms. The Trechisporales and the Corticiales were inferred to be ancestrally angiosperm-associated, while the most recent common ancestors of the Thelephorales, the Jaapiales, the Atheliales, the Gloeophyllales and the Amylocorticiales likely were associated with gymnosperms. The MRCA of the Lepidostromatales had no clear preference towards either plant groups (Supplementary Data 3). The MRCA of Agaricomycetidae was inferred to have been associated with gymnosperms (PP =

0.83), like three of the orders therein (Boletales, Amylocorticiales and Atheliales), suggesting that the evolution of these species started with a close association with gymnosperms.
By comparing the posterior probabilities of substrate preference at ancient nodes and that of extant species we found that some clades underwent remarkable changes (Supplementary Data 3). We found that the MRCA of the Polyporales, that of the Russulales and of the Boletales was likely to associated with gymnosperms (PP = 0.88, 0.98 and 0.98, respectively), yet the extant species mostly associate with angiosperms (probability of having angiosperm substrate: 0.76, 0.64 and 0.64, respectively) suggesting a major shift from gymno- to angiosperm substrates during the evolution of these clades. On the other hand, our results suggest that substrate preferences of the Corticiales, the Trechisporales and the Auriculariales have not or just slightly changed during their evolution. The posterior probability of having an angiosperm substrate was inferred as 0.84, 0.88, and 0.79 respectively at the MRCA of these clades, which is similar to the current distribution of states (0.93, 0.80 and 0.74 respectively). Interestingly, all of these orders evolved when angiosperms became the dominant component of the flora (Corticiales: 101 mya, Trechisporales: 86 mya, Auriculariales: 134 mya), therefore their angiosperm substrate preference comes as no surprise.
These results have two interesting implications. First, the ASR analyses suggest that MRCA-s of orders that originated in gymnosperm and angiosperm dominated evolutionary periods had most likely been associated with gymnosperms (Boletales, Polyporales, Russulales, Hymenochaetales and Phallomycetidae) and angiosperms (Auriculariales, Corticiales, Trechisporales) ancestrally. Second, our inferences imply that ancestrally gymnosperm-associated orders (Polyporales, Russulales and Boletales) have undergone several substrate switches during their evolution, resulting in a dominance of angiosperm association among extant members. These switches might be correlated with transitions in the global availability of gymno- vs angiosperms as substrates or hosts for fungi during the late Cretaceous period[21]. Thus, it appears that the rise of the angiosperms during the Cretaceous period left a footprint on the substrate preference of mushroom-forming fungi, an intriguing case of co-evolution driven by trophic interactions between large clades of organisms.
By analysing the overall ASR patterns through time (Figure 3/b in the main text) we found that early Agaricomycetes nodes had equally distributed probabilities between gymnosperms and angiosperms as their ancestral substrate plant group. The summed posterior probability of having had a gymnosperm substrate started to increase around 275 million years ago and reached >0.95 across all ancestors around 200 mya. This pattern coincides with the dominance of conifers in the Triassic and Jurassic period. Around 170 mya an increase in the probability of having had an angiosperm substrate was inferred. After this period, we observed a steady increase in the share of posterior probability of angiosperm substrates, with extant substrate preference distribution dominated by them too (0.32 / 0.68 = gymnosperms / angiosperms).
It should be noted, that the interpretation of inferred ancestral states of host/substrate preference has limitations for nodes older than the Permian, which predate the origin or global expansion of gymno- and angiosperms[22,23]. We found evenly distributed posterior probabilities for gymno- and angiosperms for all pre-Permian nodes, which is biologically questionable given that these weren't ubiquitously present in these periods. However, such a result is necessarily inferred in ASR analyses, because of the lack of species in our datasets that would be associated with descendants of typical Carboniferous plants (e.g. pteridophytes). Because of this methodological limitation, we had drawn conclusions from only those clades which evolved after the inferred origin of gymno- and angiosperms.

Trait dependent diversification rate analyses - The trait dependent diversification rate analyses under the BiSSE model suggest that pileate-stipitate species have higher diversification rates than non-pileate species (Supplementary Data 7, Fig. 3/e). The speciation rate for the pileate-stipitate state was 1.35–1.42 times higher than that of the non-pileate state. Model tests revealed that the unconstrained models fit the data significantly better ($p < 0.001$, LRT) than models where the two state specific rates were constrained to be equal. The extinction rate of pileate-stipitate species was 1.19–8.57 times lower than that of non-pileate species, however, in this case the unconstrained model did not fit the data significantly better than a model where the state-specific extinction rates were constrained to be equal ($\mu_0 = \mu_1$, $p > 0.05$, LRT). These results suggest that pileate-stipitate species have significantly higher speciation rates, but not significantly different extinction rates than non-pileate ones.

Supplementary Note 6.: Analyses of mass extinction events

First, we calculated Bayes factors between CoMET models with and without a mass extinction event. This analysis showed that models with a mass extinction event were preferred over models without mass extinction events (mean Bayes factor: 25.7, Supplementary Table 3.). This suggests that our data supports the presence of at least one mass extinction event during the evolution of mushroom forming fungi. To infer the number of mass extinction events and their timing, we performed rjMCMC under CoMET models with varying numbers of mass extinction events and speciation and extinction rate changes. These analyses supported one or two mass extinction events depending on the tree analyzed (Supplementary Fig. 6). This result was robust to the choice of priors on the expected number of mass extinction events, expected rate changes and survival probability (data not shown). We found that every numerical parameter reached high effective sample size values (Supplementary Table 4; ESS>500), and showed convergence according to Geweke's statistics ($p > 0.05$), except the likelihood values which, in 7 out of 10 analyses didn't pass Geweke's test although they appear converged based on the likelihood diagnostic plots. The interval specific parameters converged in every time interval (Geweke's statistics: $p > 0.05$) and had high ESS values (>500).

The results suggest that a mass extinction event happened during the Jurassic period Supplementary Fig. 6), between 200 million years ago (mya) and 145 mya, with strong support ($\ln BF > 6$) in nine out of the 10 trees. A second, a strongly supported mass extinction event was also inferred, around 230 mya, in three out of the ten trees.

Supplementary Note 7.: Latitudinal diversity gradient hypothesis

The latitudinal diversity gradient (LDG) hypothesis posits that species richness increases from the poles towards the tropics. To test this, we analyzed both centroid latitudes as continuous traits and terrestrial ecoregions as discrete traits (see Methods) for each of the species for which sufficient geographic data could be obtained (4,429 species). We fitted multiple Quantitative State Speciation and Extinction (QuaSSE) models to the ten chronograms to find the model, which best describes the latitude dependent diversification rates of Agaricomycetes species. Based on log-likelihood values, we have found that the model with Gaussian speciation and constant extinction rate fits better to our data than any other examined model and that the latitude has no effect on the extinction rate (Supplementary Table 5). These findings were supported by likelihood ratio tests, which showed that only the Gaussian speciation and constant extinction models differed significantly from the null model (constant speciation and extinction rates). Therefore, we used this model to interpolate speciation rates into a 1 × 1 degree global map (Supplementary Fig. 7). We found that the speciation rate was highest between 20° and 40° in the temperate zone. This does not coincide with the zone of the highest sampling density (30°–60°) in our data. This result suggests that latitudinal diversification patterns are largely independent from sampling patterns in our data.

In discrete analyses of geographical diversification patterns we divided all terrestrial WWF ecoregions into either tropical or extra-tropical (Supplementary Fig. 8). We assigned one of three states to each species: tropical, extra-tropical or widespread (see Materials and Methods). Using these three states for each taxon, we fitted multiple constrained models and one full model of Geographic State Speciation and Extinction (GeoSSE[24]), in a maximum-likelihood framework. The constrained models consisted of: (b) speciation in the tropics is equal to speciation in the extra-tropical zone; (c) extinction in the tropics is equal to extinction in the extra-tropical zone; (d) dispersal to the tropics occurs at the same rate as dispersal to the extra-tropical zone. The unconstrained model had the highest log-likelihood value (Supplementary Table 6), which was significantly better that the log-likelihood of any of the constrained models, based on likelihood ratio tests. In MCMC analysis we found that species in extra-tropical regions have higher diversification rate than species in tropics. (Supplementary Data 5. Interestingly in the tropics the speciation rate was higher than in the extra-tropics but so was the extinction rate. Moreover the extinction rate was near to zero in the extra-tropics which resulted in higher net diversification rate for species in extra-tropical areas.

Supplementary Note 8.: Trait independent diversification rate analyses

Accounting for non-random and incomplete taxon sampling - Taxon sampling in any phylogenetic dataset is inevitably non-random in most cases (due to how well certain groups are researched) and incomplete for large taxonomic breadths, such as Agaricomycetes. To ensure that our dataset conforms to the randomness requirement of BiSSE and BAMM models, we adjusted our taxon sampling in the 5284-taxon phylogeny. We found that 390 genera (out of 782) were significantly over- (365) or undersampled (25) based on comparisons to genus-wise diversities obtained from Species Fungorum (see Materials and Methods). We reduced the number of over- and undersampled genera to 112 and 12, respectively (complete lists are given below), by randomly removing species from oversampled genera. The remaining oversampled genera mostly contained 1 or 2 species, meaning that we couldn't mitigate oversampling without removing the genus itself from the dataset (Supplementary Data 1). The sampling fractions of pileate-stipitate and non-pileate species were 0.147 and 0.160, respectively, which means a relatively even sampling across the different states. In concordance with this, we found congruent results between different sampling bias correction strategies (built-in sampling correction, using skeletal tree or no corrections) in preliminary BiSSE and BAMM analyses (data not shown). Although we detected no obvious effect of sampling bias corrections in the results, we applied the built-in corrections of the BiSSE and BAMM models in further analyses, because we wanted to fulfill all the theoretical assumptions of the models.

Genera that remained oversampled: *Acantholichen*, *Albatrellopsis*, *Aleurobotrys*, *Allopsalliota*, *Andebbia*, *Aphroditeola*, *Atractosporocybe*, *Australovuilleminia*, *Barcheria*, *Basidioradulum*, *Bertrandia*, *Biatoropsis*, *Bogbodia*, *Bondarcevomyces*, *Bothia*, *Botryohypochnus*, *Brunneocorticium*, *Bulbillomyces*, *Calocybella*, *Calvarula*, *Cantharellopsis*, *Caripia*, *Catatrama*, *Cibaomyces*, *Claustula*, *Coniolepiota*, *Crustodontia*, *Dendrocollybia*, *Dentipellopsis*, *Dictyopanus*, *Earliella*, *Eonema*, *Ertzia*, *Faerberia*, *Fevansia*, *Flavophlebia*, *Gastrocybe*, *Giacomia*, *Gigasperma*, *Globulicium*, *Globulisebacina*, *Gloeostereum*, *Granulobasidium*, *Guyanagaster*, *Gymnogaster*, *Gyrodontium*, *Haloaleurodiscus*, *Halocyphina*, *Hebelomina*, *Heinemannomyces*, *Heliocybe*, *Hemistropharia*, *Hydnomerulius*, *Hymenogloea*, *Kauffmania*, *Kjeldsenia*, *Laeticorticium*, *Laeticutis*, *Lampteromyces*, *Lepistella*, *Leucocortinarius*, *Limnoperdon*, *Mackintoshia*, *Mayamontana*, *Melanoporia*, *Membranomyces*, *Mycobonia*, *Mycopan*, *Myriostoma*, *Mythicomyces*, *Naiadolina*, *Neohygrophorus*, *Neolentiporus*, *Nothocastoreum*, *Notholepista*, *Ossicaulis*, *Paragyrodon*, *Paulisebacina*, *Phaeolepiota*, *Phaeomyces*, *Phallobata*, *Phylloboletellus*, *Piptoporus*, *Pirex*, *Polyozellus*, *Polypus*, *Porodisculus*, *Porpolomopsis*, *Protoxerula*, *Pseudohydnum*, *Pterulicium*, *Pulcherricium*, *Rhopalogaster*, *Richoniella*, *Royoungia*, *Sarcomyxa*, *Solioccasus*, *Sparsitubus*, *Sphagnurus*, *Stagnicola*, *Stromatoscypha*, *Sulzbacheromyces*, *Tephrocybella*, *Terana*, *Termiticola*, *Torrendia*, *Trametopsis*, *Tremellogaster*, *Tricholomella*, *Tsuchiyaea*, *Woldmaria*, *Xanthoporia*

Undersampled genera: *Clitocybe* s.l., *Clitopilus*, *Collybia*, *Ganoderma*, *Lachnella*, *Marasmiellus*, *Marasmius*, *Mycena*, *Peniophora*, *Russula*, *Tomentella*, *Tyromyces*

Trait independent diversification rate analyses - In BAMM analyses, all parameters converged to stationary values within the specified burn-in phase of the runs, based on diagnostic plots (Supplementary Fig. 9) and Geweke's diagnostics ($p > 0.05$). Despite the extremely long MCMC

chains (100 million generations), however, ESS values were moderate (< 200) for some of the parameters (Supplementary Table 7).

Detecting evolutionary rate shifts in Agaricomycetes evolution - After discarding the first 50 million generations as burn-in, we obtained 5001 samples from the posterior. Because virtually every posterior sample comprised a unique shift configuration (due to the size of the phylogeny being analyzed), we decided to focus on core shifts that are taxonomically and statistically consistent across >4 out of 10 chronograms, termed here congruent core shifts (for definition see the methods). After excluding non-congruent and mutually exclusive core shifts, we obtained 85 congruent core shifts (Supplementary Data 5). By calculating the cumulative posterior probability of the congruent core shifts as a function of generations we found that the posterior probabilities of each of the congruent core shifts were converged (Supplementary Fig. 9). Congruent core shifts were detected in several clades across the entire tree (Supplementary Data 5). We inferred congruent core shifts in the MRCA of many order-level clades, including the Tremellomycetes, the Dacrymycetes, the Cantharellales, the Sebacinales, the Auriculariales, the Hymenochaetales and Agaricales. In the Hymenochaetales, the shift was inferred in the MRCA of most species of the order, to the exception of the Repetobasidiaceae. Deeper in the tree, we detected rate shifts in the MRCA of each of the Phallomycetidae, Agaricomycetidae, the monophyletic group formed by Russulales, Polyporales, Thelephorales, Corticiales, Gloeophyllales and Jaapiales and the clade formed by Boletales, Amylocorticiales, Lepidostromatales and Atheliales. Most of the congruent core shifts were inferred in Agaricales (57). Also, all but 15 of them were associated with an increase in net diversification rate, indicating accelerated diversification.

Diversification rate changes through time - By analysing rates through time we found that net diversification rate started to increase between 197–163 mya in the Jurassic period (Fig. 2). To examine if this was a tree-wide pattern or was caused by a single or a few orders, we re-calculated rates through time by iteratively eliminating each of the orders and the Agaricomycetidae from the tree. This analysis showed that in most of the trees the signals did not disappear by excluding certain order or higher-level group (Fig. 2), suggesting that the Jurassic acceleration of diversification rate happened across the entire Agaricomycetes.
The main contributor to this pattern was speciation rate (Fig. 2). The acceleration of speciation rate was followed by an increase in extinction rate (195–125 Mya), consistent with the finding of potential mass extinction events (Fig. 2, Supplementary Fig. 6, Supplementary note 6).

Validation of BAMM estimates - Because BAMM's diversification estimates received criticism recently, we analyzed our data using a complementary approach as well. We found that the estimated evolutionary rates were congruent across the two methods and different settings (Supplementary Fig. 10, Supplementary Table 8; adjusted R squared: 0.41–0.60 and $p < 0.001$). The method-of-moments (MS) approach estimated lower diversification rate values relative to BAMM (Supplementary Fig. 10). In general, the MS estimates fit better to BAMM's diversification rates than to speciation rates. Furthermore, MS estimates obtained with crown ages generally fit better to BAMM data than those obtained with stem ages. The latter result was expected since BAMM estimates are based on only crown ages. Also, MS models without extinction rates ($\varepsilon = 0$) fit better to BAMM data than models with any extinction fractions (Supplementary Table 8). Altogether the two methods estimated similar mean diversification rates of clades, suggesting that our results are robust across different methods with different assumptions.

Supplementary Figures

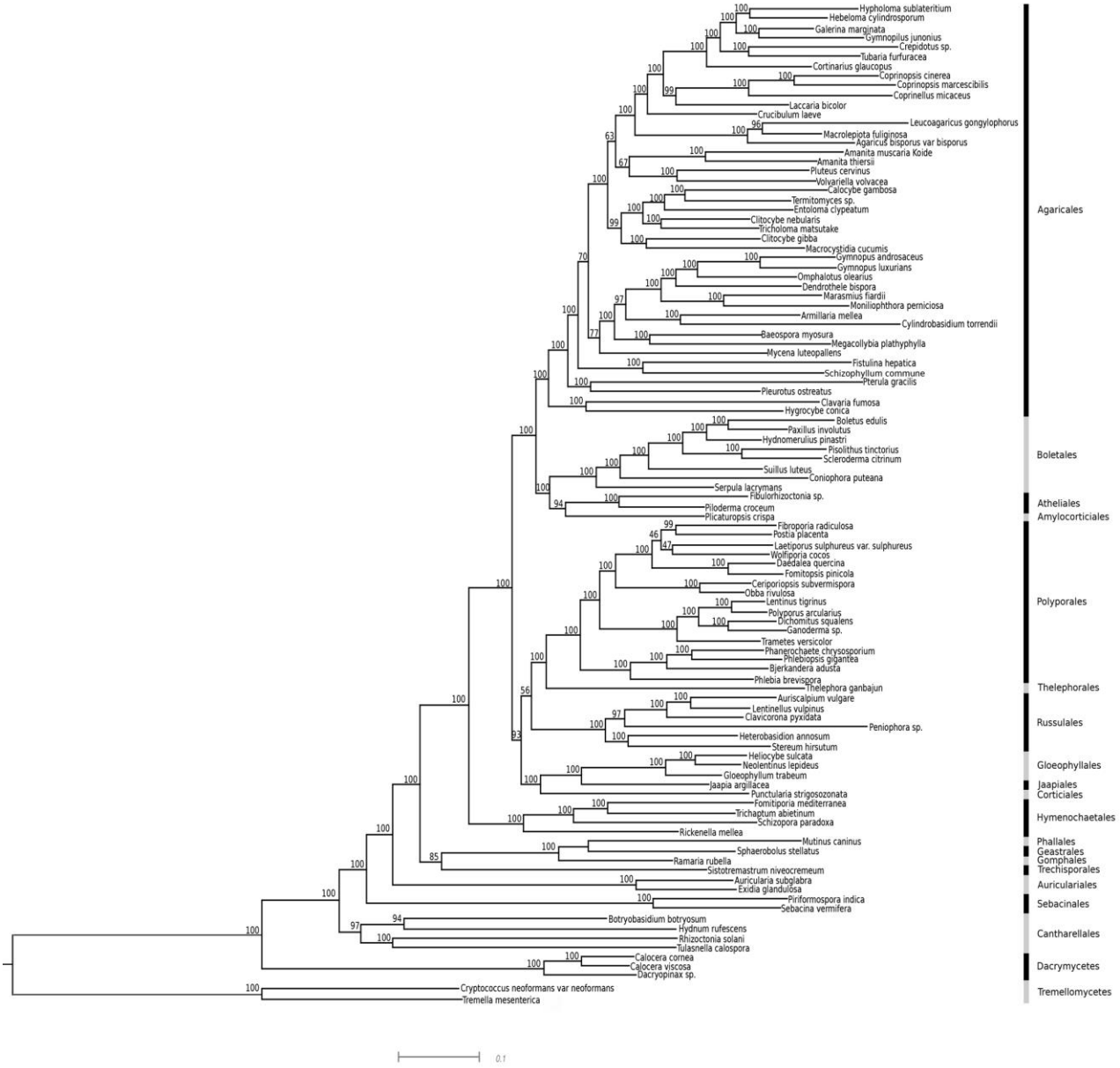

Supplementary Figure 1. Higher-level phylogenomic relationships of Agaricomycotina. Maximum-likelihood phylogenetic tree inferred from a supermatrix containing 141,951 amino acid sites partitioned into 650 genes from 104 genomes using RAxML under the PROTGAMMAWAG model. Numbers next to branches indicate the percent support from 100 nonparametric bootstraps. This phylogenomic tree was used as a topological constrain in the ML analysis of the 5284-species dataset.

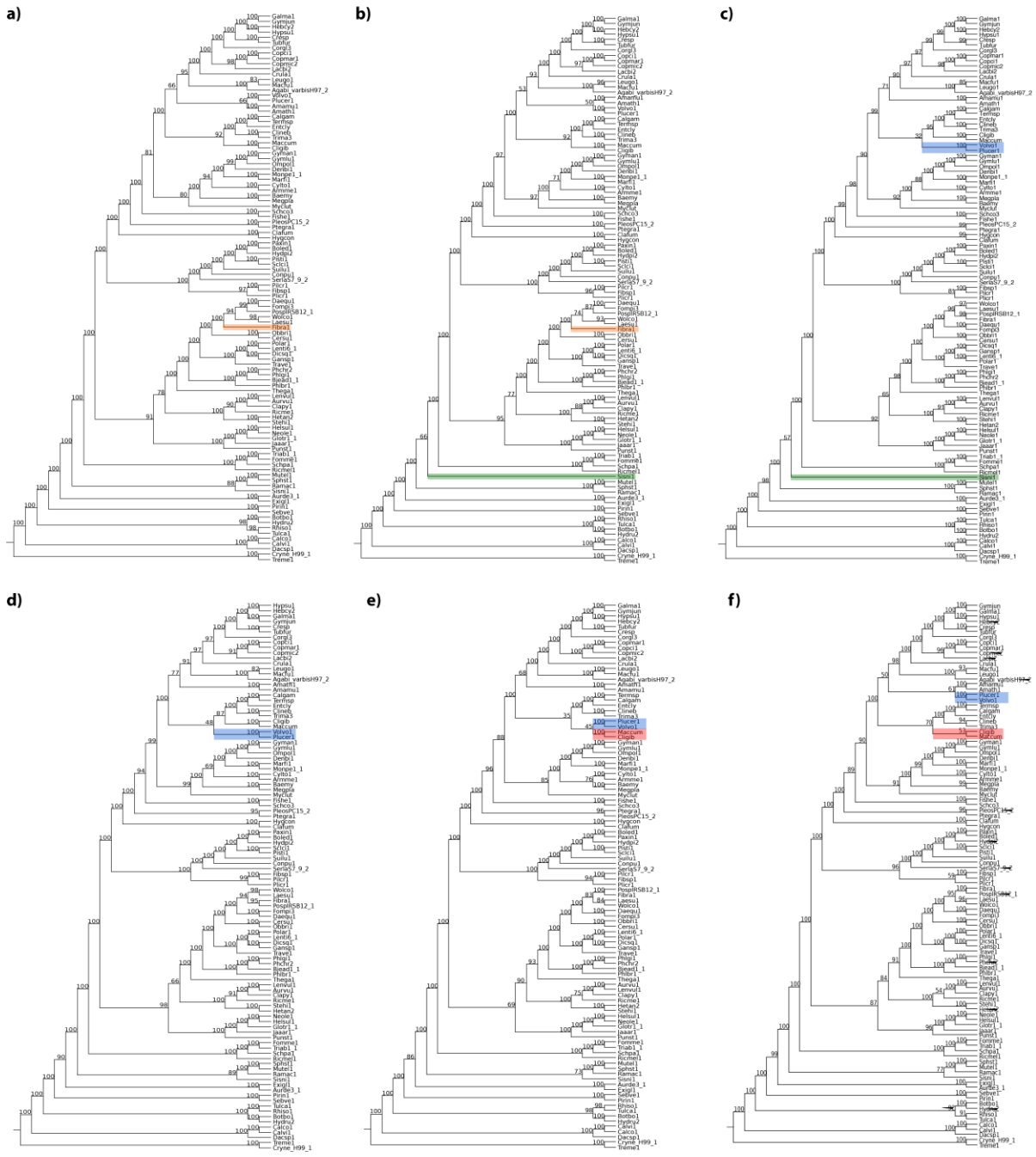

Supplementary Figure 2. Sensitivity analyses addressing the robustness of phylogenomic analyses. Maximum-likelihood trees inferred by progressively removing fast-evolving sites using Gblocks. Maximum Likelihood trees inferred from trimmed concatenated matrices containing 129.886 (A), 107.496 (B), 89.732 (C), 76.153 (D), 70.862 (E) and 63.309 (F) amino acid cites. Changes in topology affect the weekly supported branches shown by colored panels: *Fibroporia radiculosa* (Fibra1; orange) (A, B) and *Sistotremastrum niveocremeum* (Sisni1; green) (B, C), Pluteaceae (Plucer1, Volvo1; blue) (C-F) and Macrocystidiaceae (Cligib, Maccum; purple) (E,F).

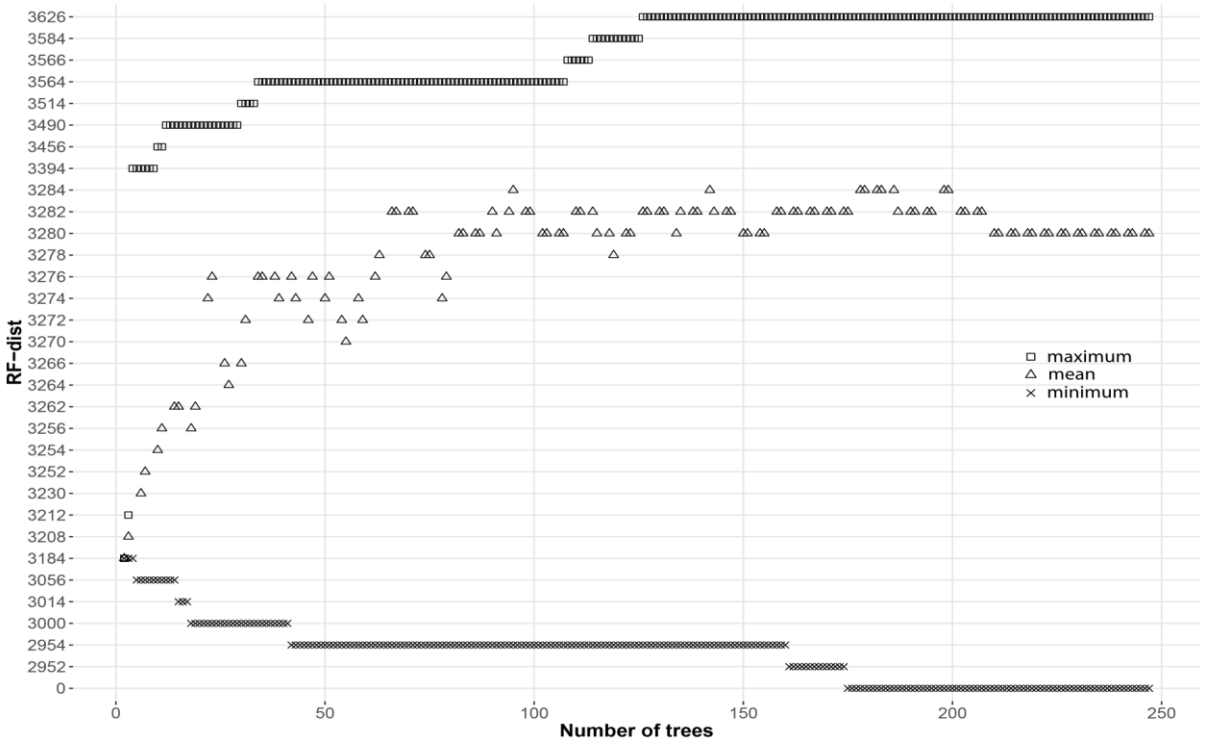

Supplementary Figure 3. The saturation of RF-distance values as a function of the number of ML trees. With increasing the number of trees the maximum, minimum and the average of pair-wise Robinson-Foulds distances are saturated.

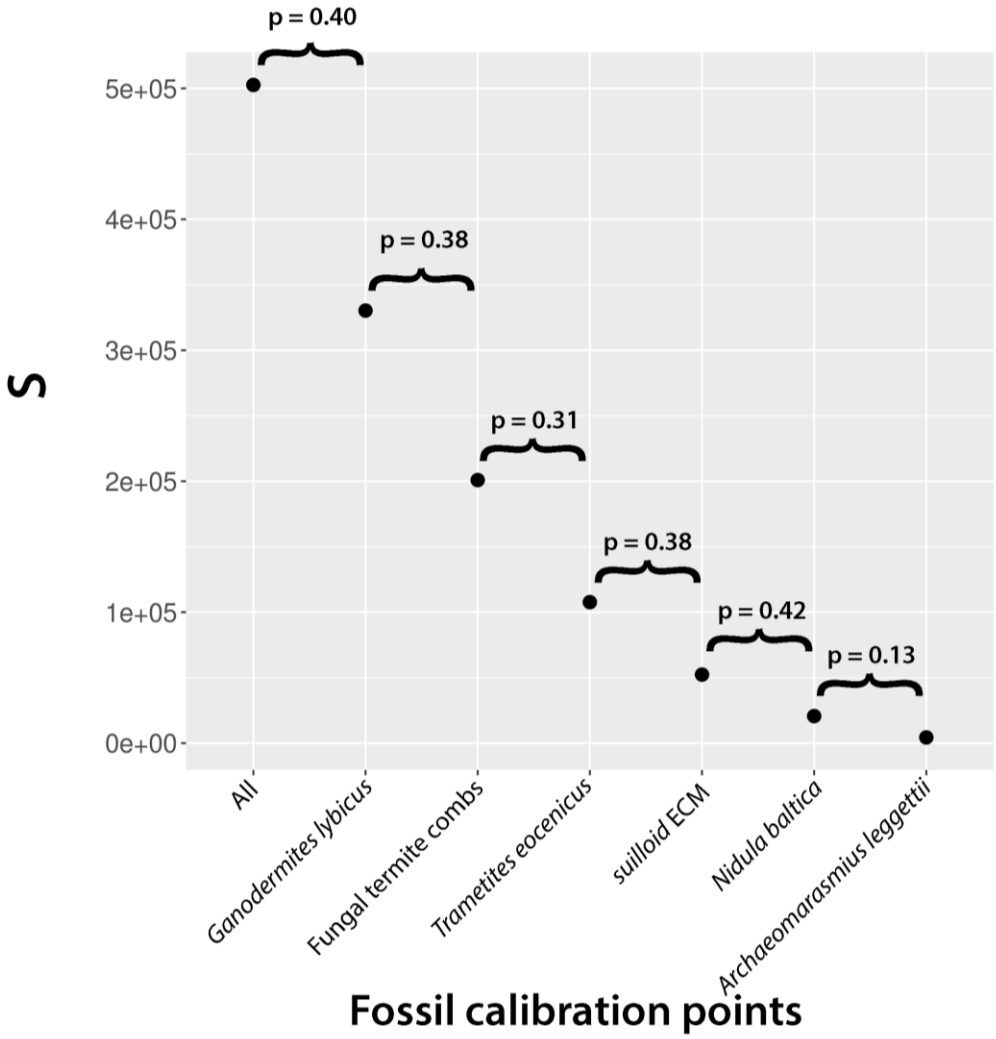

Supplementary Figure 4. The effects of removing fossil calibration points on the average squared deviation (*s*) between molecular and fossil age estimates for all calibration points. We conclude that fossil calibration points (listed in Supplementary Table 2) are not conflicting with each other because by removing a fossil calibration point *s* is decreased by an insignificant value, and there was no significant drop in the variance of *s* (one-tailed F-test, $p<0.05$) in any one comparison.

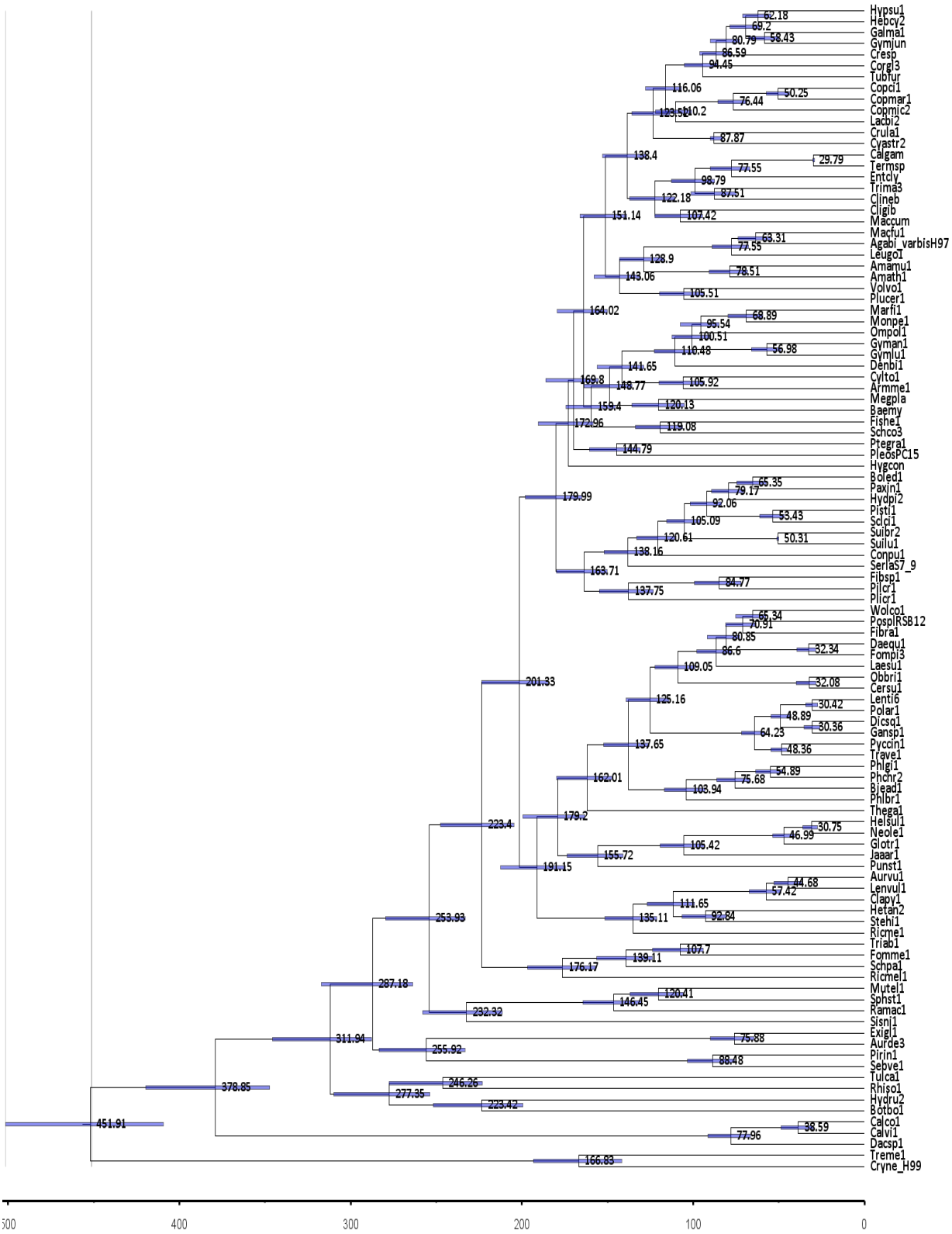

Supplementary Figure 5. Time calibrated chronogram inferred using mcmctree for the 105-species phylogenomic dataset. Numbers at nodes represent mean ages, bars are depict 95% highest posterior densities (HPD). For genome description see Supplementary Table 1.

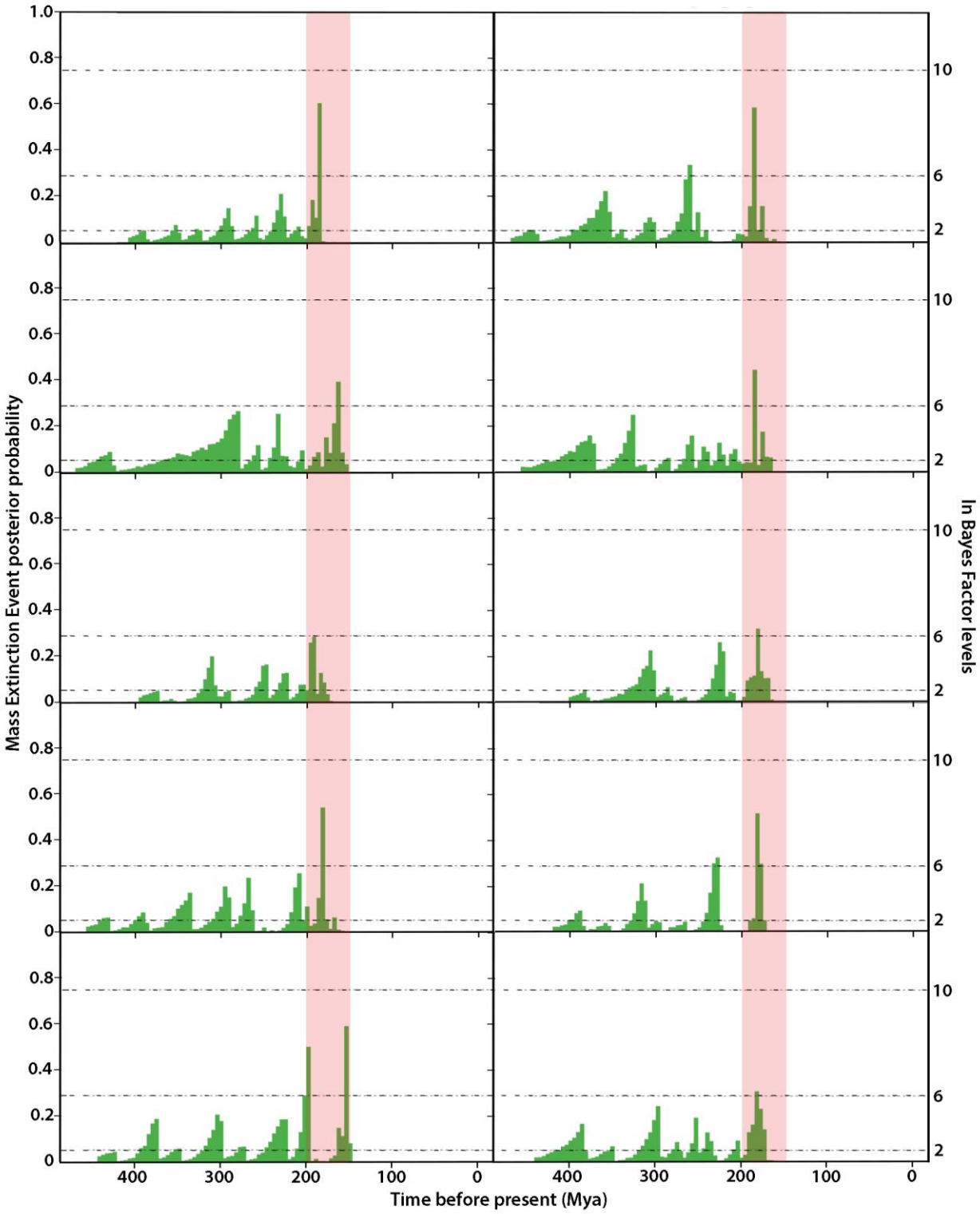

Supplementary Figure 6. Inferred mass extinction events. The left y-axis represents the posterior probability of a mass extinction event in a given time frame. Dashed lines indicate ln Bayes factor thresholds of significance. We considered ln Bayes factor>6 as strong support for an event (right y-axis). The 10 graphs represent the results for 10 analyzed chronograms. Shaded red region shows the interval of the Jurassic period.

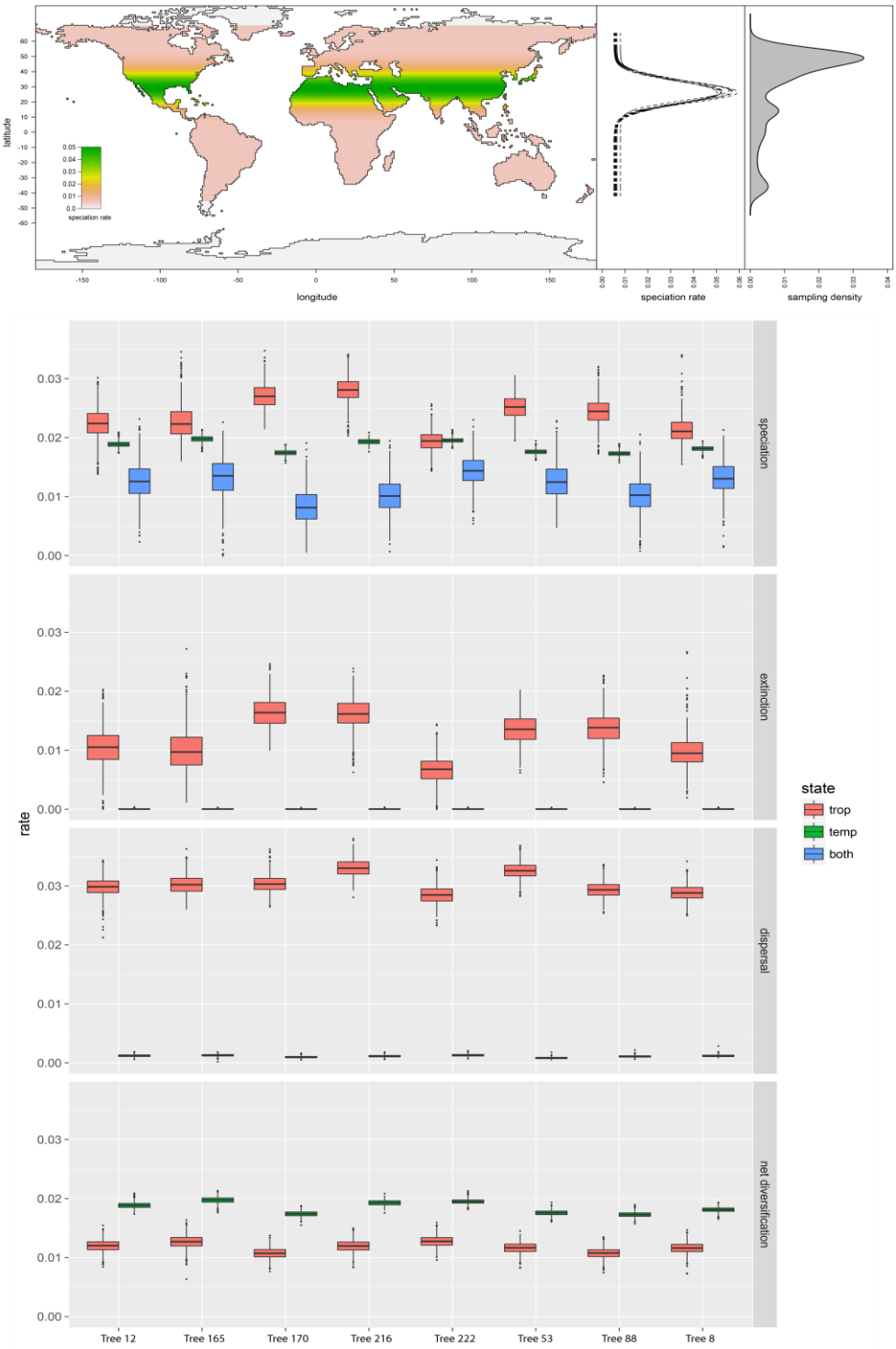

Supplementary Figure 7. Results of analyses of the latitudinal diversity gradient hypo-thesis. Upper panel shows the speciation rates in a 1 x 1 degree global map inferred under Quantitative State Speciation and Extinction (QuaSSE) model. On the right the distribution of the inferred speciation rates and the sampling density are shown along the latitudinal positions. Note that the sampling density doesn't overlap with the distribution of speciation rate. Lower panel shows the distribution of inferred rates using the Geographic State Speciation and Extinction (GeoSSE) model.

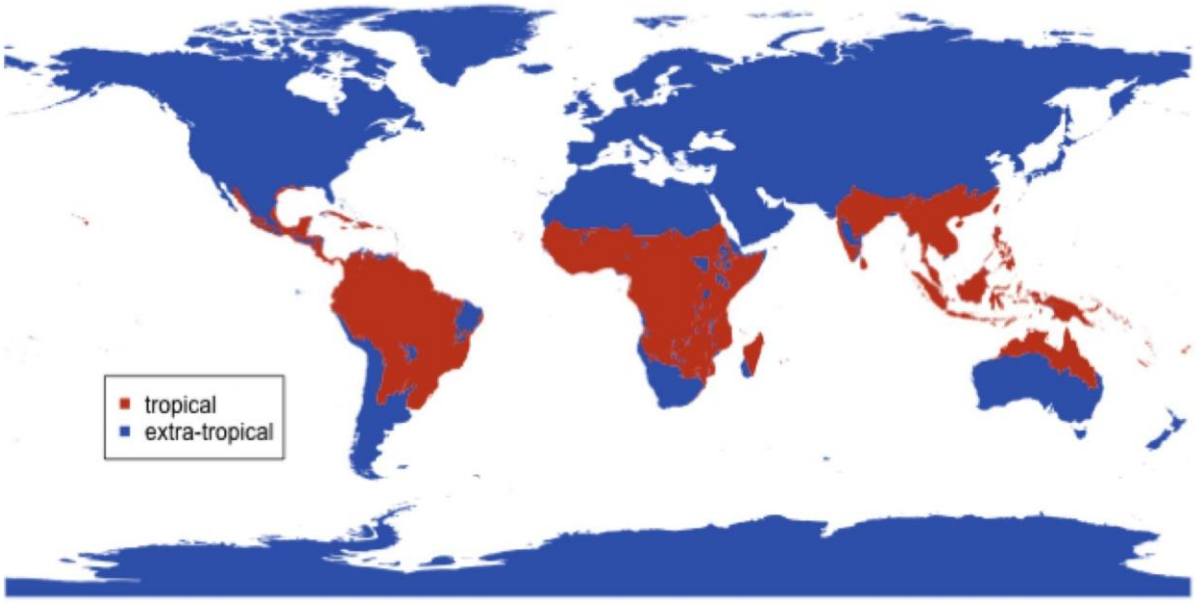

Supplementary Figure 8. The tropical and extra-tropical eco-regions

a)

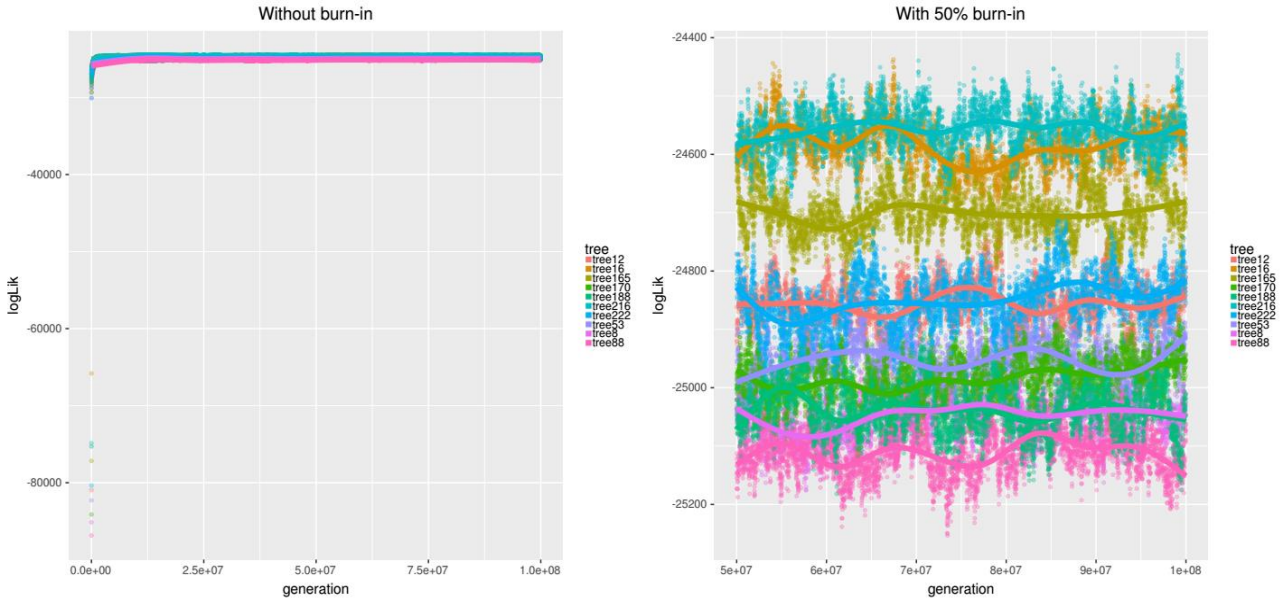

b)

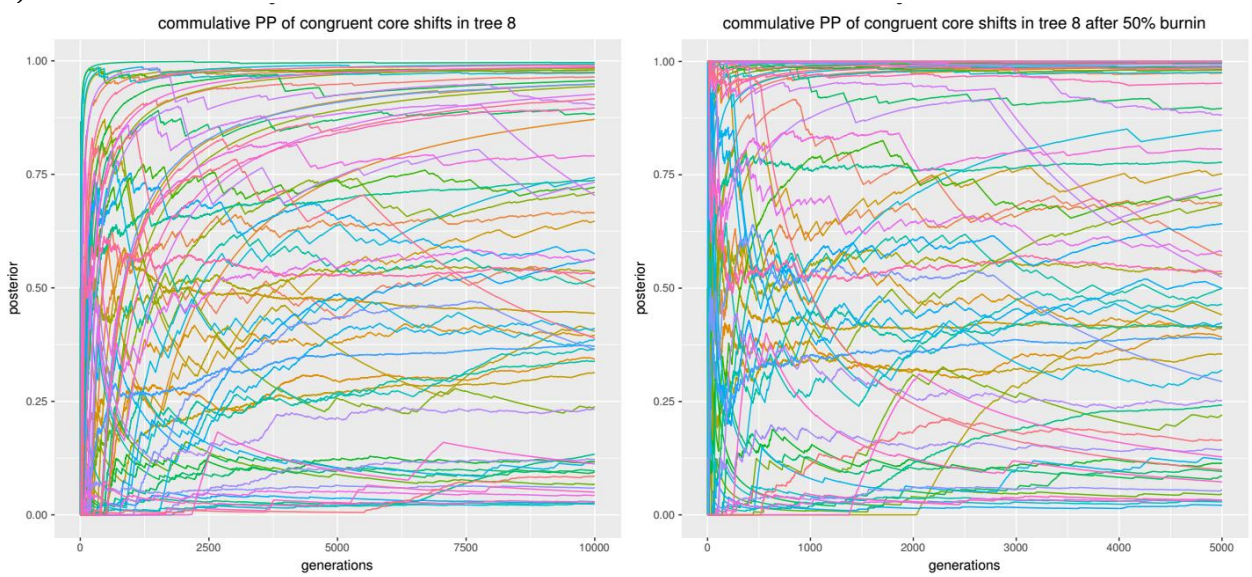

Supplementary Figure 9. a) The convergence of log likelihood values during the BAMM analyses. b) Cumulative posterior probability of congruent core shifts found in the BAMM analysis of tree 8. Left panel plots all samples obtained during the analysis; right panel shows only post-burn-in samples.

a)

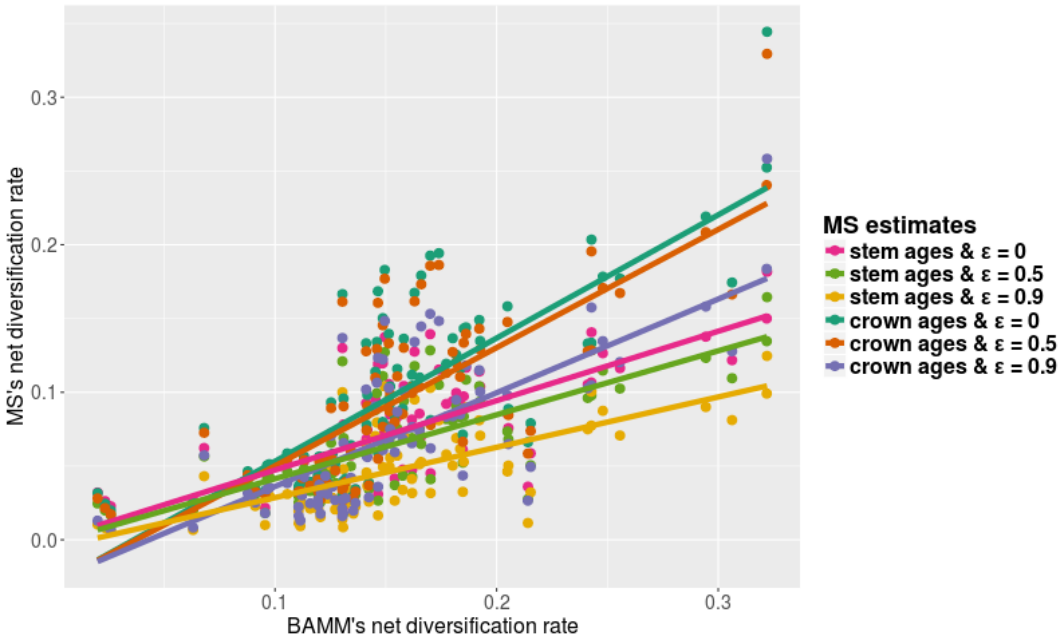

b)

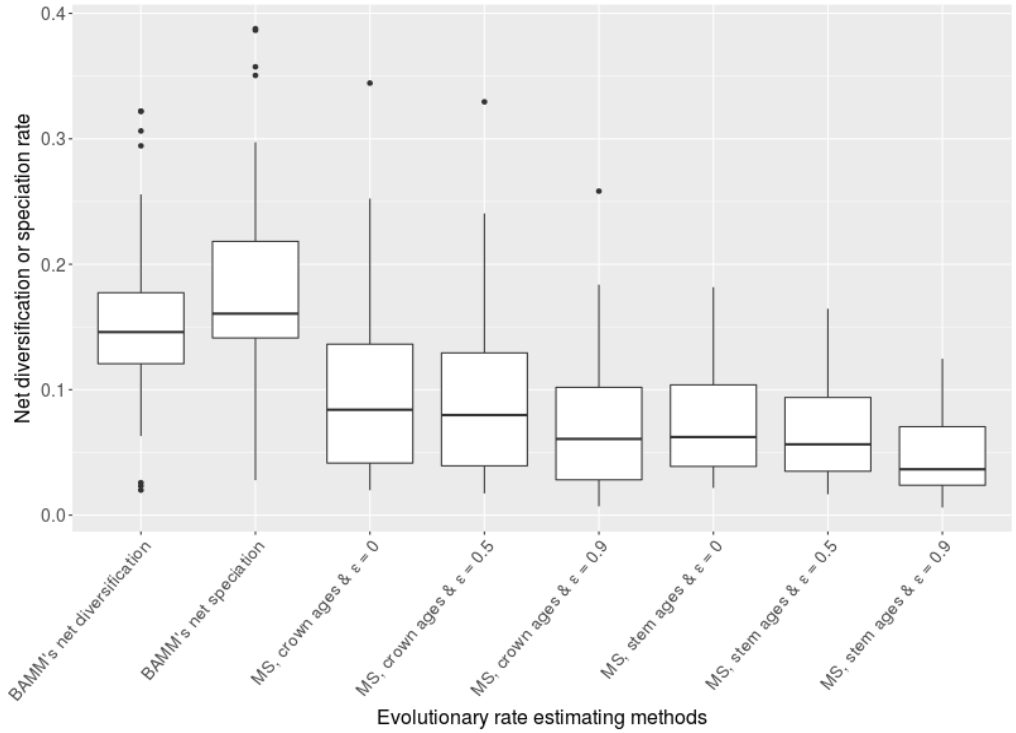

Supplementary Figure 10. a) Correlation between net diversification rate estimates by BAMM's and the MS method under various settings. ε = relative extinction rate. b) Comparison of results of BAMM and MS diversification rate estimates based on the average rates of 85 clades that subtend congruent core shifts. ε = relative extinction rate.

Supplementary Tables

Supplementary Table 1. Genomes used in this study. New genomes are in bold.

Species	Abbreviation	Order	Family	References
Agaricus bisporus var bisporus H97	Agabi_varbisH97_2	Agaricales	Agaricaceae	Morin et al.[25]
Amanita muscaria Koide	Amamu1	Agaricales	Amanitaceae	Kohler et al.[6]
Amanita thiersii	Amath1	Agaricales	Amanitaceae	Wolfe et al.[26]
Armillaria mellea	Armme1	Agaricales	Physalacriaceae	Collins et al.[27]
Auricularia subglabra	Aurde3_1	Auriculariales	Auriculariaceae	Floudas et al.[28]
Auriscalpium vulgare	Aurvu1	Russulales	Auriscalpiaceae	L. G. Nagy
Baeospora myosura	Baemy	Agaricales	Cyphellaceae*	B. T. M. Dentinger
Bjerkandera adusta	Bjead1_1	Polyporales	Meruliaceae (phlebioid clade[#])	Binder et al.[11]
Boletus edulis	Boled1	Boletales	Boletaceae	F. Martin
Botryobasidium botryosum	Botbo1	Cantharellales	Botryobasidiaceae	Riley et al.[29]
Calocera cornea	Calco1	Dacrymycetales	Dacrymycetaceae	Nagy et al.[5]
Calocybe gambosa	Calgam	Agaricales	Lyophyllaceae	B. T. M. Dentinger
Calocera viscosa	Calvi1	Dacrymycetales	Dacrymycetaceae	Nagy et al.[5]
Ceriporiopsis (Gelatoporia) subvermispora	Cersu1	Polyporales	gelatoporia clade[#]	Fernandez-Fueyo et al.[30]
Clavaria fumosa	Clafum	Agaricales	Clavariaceae	B. T. M. Dentinger
Clavicorona pyxidata (*Artomyces pyxidatus*)	Clapy1	Russulales	Auriscalpiaceae	L. G. Nagy
Clitocybe gibba (*Infundibulicybe gibba*)	Cligib	Agaricales	Tricholomataceae	B. T. M. Dentinger
Clitocybe nebularis	Clineb	Agaricales	Tricholomataceae	B. T. M. Dentinger
Coniophora puteana	Conpu1	Boletales	Coniophoraceae	Floudas et al.[7]
Coprinopsis cinerea	Copci1	Agaricales	Psathyrellaceae	Stajich et al.[31]
Coprinopsis marcescibilis	**Copmar1**	**Agaricales**	**Psathyrellaceae**	**This study**
Coprinellus micaceus	**Copmic2**	**Agaricales**	**Psathyrellaceae**	**This study**
Cortinarius glaucopus	Corgl3	Agaricales	Cortinariaceae *s str.**	F. Martin
Crepidotus sp.	Cresp	Agaricales	Crepidotaceae*	B. T. M. Dentinger
Crucibulum laeve	**Crula1**	**Agaricales**	**Nidulariaceae***	**This study**
Cryptococcus neoformans var neoformans	Cryne_H99_1	Tremellales	Tremellaceae	Janbon et al.[32]
Cylindrobasidium torrendii	Cylto1	Agaricales	Physalacriaceae	Floudas et al.[15]
Dacryopinax sp.	Dacsp1	Dacrymycetales	Dacrymycetaceae	Floudas et al.[7]
Daedalea quercina	Daequ1	Polyporales	Fomitopsidaceae (antrodia clade[#])	Nagy et al.[5]
Dendrothele bispora	**Denbi1**	**Agaricales**	**Corticiaceae**	**This study**
Dichomitus squalens	Dicsq1	Polyporales	Polyporaceae (core polyporoid clade[#])	Floudas et al.[7]
Entoloma clypeatum	Entcly	Agaricales	Entolomataceae	B. T. M. Dentinger
Exidia glandulosa	Exigl1	Auriculariales	Auriculariaceae	Nagy et al.[5]
Fibroporia radiculosa	Fibra1	Polyporales	Fomitopsidaceae (antrodia clade[#])	Tang et al.[33]
Fibulorhizoctonia sp.	Fibsp1	Atheliales	Atheliaceae	Nagy et al.[5]
Fistulina hepatica	Fishe1	Agaricales	Schizophyllaceae*	Floudas et al.[15]
Fomitiporia mediterranea	Fomme1	Hymenochaetales	Hymenochaetaceae	Floudas et al.[7]
Fomitopsis pinicola	Fompi3	Polyporales	Fomitopsidaceae (antrodia clade[#])	Floudas et al.[7]

Galerina marginata	Galma1	Agaricales	Hymenogastraceae	Riley et al.[29]
Ganoderma sp.	Gansp1	Polyporales	Ganodermataceae (core polyporoid clade[#])	Binder et al.[11]
Gloeophyllum trabeum	Glotr1_1	Gloeophyllales	Gloeophyllaceae	Floudas et al.[7]
Gymnopus androsaceus	Gyman1	Agaricales	Omphalotaceae	F. Martin
Gymnopilus junonius	Gymjun	Agaricales	Gymnopileae*	B. T. M. Dentinger
Gymnopus luxurians	Gymlu1	Agaricales	Omphalotaceae	Kohler et al.[6]
Hebeloma cylindrosporum	Hebcy2	Agaricales	Hymenogastraceae	Kohler et al.[6], Dore et al.[34]
Heliocybe sulcata	**Helsul1**	**Gloeophyllales**	**Gloeophyllaceae**	**This study**
Heterobasidion annosum	Hetan2	Russulales	Bondarzewiaceae	Olson et al.[35]
Hydnomerulius pinastri	Hydpi2	Boletales	Paxillaceae	Kohler et al.[6]
Hydnum rufescens	Hydru2	Cantharellales	Hydnaceae	Francis Martin
Hygrocybe conica	Hygcon	Agaricales	Hygrophoraceae	B. T. M. Dentinger
Hypholoma sublateritium	Hypsu1	Agaricales	Strophariaceae *s str.**	Kohler et al.[6]
Jaapia argillacea	Jaaar1	Jaapiales	Jaapiaceae	Riley et al.[29]
Laccaria bicolor	Lacbi2	Agaricales	Hydnangiaceae	Martin et al.[36]
Laetiporus sulphureus var. *sulphureus*	Laesu1	Polyporales	Fomitopsidaceae (antrodia clade[#])	Nagy et al.[5]
Lentinus tigrinus	Lenti6_1	Polyporales	Polyporaceae (core polyporoid clade[#])	D. Hibbett
Lentinellus vulpinus	Lenvul1	Russulales	Auriscalpiaceae	L. G. Nagy
Leucoagaricus gongylophorus	Leugo1	Agaricales	Agaricaceae	Aylward et al.[37]
Macrocystidia cucumis	Maccum	Agaricales	Macrocystidiaceae*	B. T. M. Dentinger
Macrolepiota fuliginosa	Macfu1	Agaricales	Agaricaceae	F. Martin
Marasmius fiardii	Marfi1	Agaricales	Marasmiaceae	F. Martin
Megacollybia plathyphylla	Megpla	Agaricales	hydropoid clade*	B. T. M. Dentinger
Moniliophthora perniciosa	Monpe1_1	Agaricales	Marasmiaceae	Mondego et al.[38]
Mutinus caninus	Mutel1	Phallales	Phallaceae	P. Crous
Mycena luteopallens	Myclut	Agaricales	Mycenaceae	B. T. M. Dentinger
Neolentinus lepideus	Neole1	Gloeophyllales	Gloeophyllaceae	Nagy et al.[5]
Obba rivulosa	Obbri1	Polyporales	gelatoporia clade[#]	Miettinen et al.[39]
Omphalotus olearius	Ompol1	Agaricales	Omphalotaceae	Wawrzyn et al.[40]
Paxillus involutus	Paxin1	Boletales	Paxillaceae	Kohler et al.[6]
***Peniophora* sp.**	**Ricme1**	**Russulales**	**Peniophoraceae**	**Nagy et al.**[5]
Phanerochaete chrysosporium	Phchr2	Polyporales	Phanerochaetaceae (phlebioid clade[#])	Ohm et al.[41]
Phlebia brevispora	Phlbr1	Polyporales	Phanerochaetaceae (phlebioid clade[#])	Binder et al.[11]
Phlebiopsis gigantea	Phlgi1	Polyporales	Phanerochaetaceae (phlebioid clade[#)]	Hori et al.[42]
Piloderma croceum	Pilcr1	Atheliales	Atheliaceae	Kohler et al.[6]
Piriformospora indica	Pirin1	Sebacinales		Zuccaro et al.[43]
Pisolithus tinctorius	Pisti1	Boletales	Sclerodermataceae	Kohler et al.[6]
Pleurotus ostreatus	PleosPC15_2	Agaricales	Pleurotaceae	Riley et al.[29], Castanera et al.[44], Alfaro et al.[45]
Plicaturopsis crispa	Plicr1	Amylocorticiales	Amylocorticiaceae	Kohler et al.[6]
Pluteus cervinus	**Plucer1**	**Agaricales**	**Pluteaceae**	**This study**
Polyporus arcularius	**Polar1**	**Polyporales**	**Polyporaceae (core polyporoid clade[#])**	**This study**

Postia placenta	PosplRSB12_1	Polyporales	Polyporaceae(antrodia clade[#])	Martinez et al.[46]
Pterula gracilis	**Ptegra1**	**Agaricales**	**Pterulaceae**	**This study**
Punctularia strigosozonata	Punst1	Corticiales	Punctulariaceae	Floudas et al.[7]
Ramaria rubella	Ramac1	Gomphales	Gomphaceae	F. Martin
Rhizoctonia solani	Rhiso1	Cantharellales	Ceratobasidiaceae	Wibberg et al.[47]
Rickenella mellea	Ricmel1	Hymenochaetales	Repetobasidiaceae	L. G. Nagy
Schizophyllum commune	Schco3	Agaricales	Schizophyllaceae	J. Stephen Horton
Schizopora paradoxa	Schpa1	Hymenochaetales	Schizoporaceae	Min et al.[48]
Scleroderma citrinum	Sclci1	Boletales	Sclerodermataceae	Kohler et al.[6]
Sebacina vermifera	Sebve1	Sebacinales		Kohler et al.[6]
Serpula lacrymans	SerlaS7_9_2	Boletales	Serpulaceae	Eastwood et al.[49]
Sistotremastrum niveocremeum	Sisni1	Trechisporales	Hydnodontaceae	Nagy et al.[5]
Sphaerobolus stellatus	Sphst1	Geastrales	Geastraceae	Kohler et al.[6]
Stereum hirsutum	Stehi1	Russulales	Stereaceae	Floudas et al.[7]
Suillus luteus	Suilu1	Boletales	Suillaceae	Kohler et al.[6]
Termitomyces sp.	Termsp	Agaricales	Lyophyllaceae	B. T. M. Dentinger
Thelephora ganbajun	Thega1	Thelephorales	Telephoraceae	P. Wang
Trametes versicolor	Trave1	Polyporales	Polyporaceae (core polyporoid clade[#])	Floudas et al.[7]
Tremella mesenterica Fries	Treme1	Tremellales	Tremellaceae	Floudas et al.[7]
Trichaptum abietinum	Triab1_1	Hymenochaetales		L. G. Nagy
Tricholoma matsutake	Trima3	Agaricales	Tricholomataceae	F. Martin
Tubaria furfuracea	Tubfur	Agaricales	Tubariae*	B. T. M. Dentinger
Tulasnella calospora	Tulca1	Cantharellales	Tulsanellaceae	Kohler et. al[6]
Volvariella volvacea	Volvo1	Agaricales	Pluteaceae	Bao et al.[50]
Wolfiporia cocos	Wolco1	Polyporales	Polyporaceae (antrodia clade[#])	Floudas et al.[7]

*Classification based on Matheny et al.[14]
Binder et al.[11]

Supplementary Table 2. Nine calibration points used in molecular dating of phylogenetic trees. An age constraint was further applied to the root because molecular age estimation methods generally poorly resolve root ages. All calibration points define the crown node of each group listed here.

Fossil	**Calibration point**	**Mininum Age (myr)**	**Maximum Age (myr)**	**Reference**
Quatsinoporites cranhamii	Hymenochaetales	127	250	Smith et al.[51]
Ganodermites lybicus	Ganoderma	18	50	Fleischmann et al.[52]
Archaemarasmius legettii	marasmioid clade	92	180	Hibbett et al.[53]
Palaeoagaricites antiquus	Agaricales	105	210	Poinar & Buckley[54]
Nidula baltica	Nidulariaceae	45	90	Poinar[55]
Suilloid ECM	Suillaceae	50	100	Lepage et al.[56]
Fungal termite combs	Termitomyces	7	30	Duringer et al.[57]
Trametites eocenicus	Trametes	45	90	Knobloch & Kotlaba[58]
	Root	300	600	

Supplementary Table 3. Results of MCMC analyses under models with and without mass extinction events. The null model (M_0) was a constant-rate birth-death CoMET model with mass extinction events allowed and the alternative model (M_1) was the same as M_0 but without a mass extinction event. Bayes factors were calculated from the marginal likelihoods of the two models, using stepping stone simulation.

Tree analyzed	Marginal log likelihood values		Bayes Factor
	Mass extinction	No mass extinction	
8	-24116	-24128	23
12	-23930	-23947	34
16	-23543	-23554	21
53	-23826	-23838	25
88	-24032	-24043	22
165	-23638	-23648	21
170	-24049	-24065	31
188	-24058	-24071	26
216	-23480	-23494	27
222	-23937	-23951	27

Supplementary Table 4. Convergence statistics of numerical parameters in rjMCMC analyses of CoMET models.

Trees	**log likelihood**			**# of Speciation rate shifts**			**# of Extinction rate shifts**			**# of Mass extinction events**		
	Mean	ESS	Geweke statistics	Mean	ESS	Geweke statistics	Mean	ESS	Geweke statistics	Mean	ESS	Geweke statistics
Tree 8	-23844	2108	sig.	30	2224	non sig.	29	1806	non sig.	3.4	2275	non sig.
Tree 12	-23646	2251	non sig.	30	2251	non sig.	27	1842	non sig.	4.4	2251	non sig.
Tree 16	-23241	2119	non sig.	30	2251	non sig.	30	1797	non sig.	5.4	2295	non sig.
Tree 53	-23449	2251	non sig.	30	2103	non sig.	28	1733	non sig.	4.6	1778	non sig.
Tree 88	-23638	922	sig.	29	2251	non sig.	28	1354	non sig.	3.2	2185	non sig.
Tree 165	-23301	2251	sig.	30	2251	non sig.	27	1541	non sig.	3.7	2251	non sig.
Tree 170	-23726	2251	sig.	30	2251	non sig.	28	1363	non sig.	4.4	1960	non sig.
Tree 188	-23685	1113	sig.	30	2251	sig.	28	2072	non sig.	3.7	2251	non sig.
Tree 216	-23106	2251	sig.	30	2251	non sig.	29	1895	non sig.	5.1	2251	non sig.
Tree 222	-23671	1641	sig.	30	2251	non sig.	28	1848	non sig.	4.3	2251	non sig.

Supplementary Table 5. QuaSSE model fit. Values are averaged across 10 trees. dAIC is the AIC differences between the best and other models. lnL is the ln-likelihood of the given model.

Model	Df	lnL	AIC	dAIC	p-value
Constant speciation and extinction	3	-50732.2	101470.5	949.8	--
Gaussian speciation and const. extinction	**6**	**-50254.3**	**100520.7**	**0**	**<2e-16 *****
Linear speciation and const. extinction	4	-50732.1	101472.4	951.7	0.59
Const. speciation and linear extinction	4	-50732.2	101472.4	951.7	0.84
Const. speciation and Gaussian extinction	6	-50732.1	101476.2	955.5	0.93

Supplementary Table 6. GeoSSE model fit. Values are averaged across 10 trees. dAIC is the AIC differences between the best and other models. lnL is the ln-likelihood of the given model.

Model	Df	lnL	AIC	dAIC	p-value
full	**7**	**-28232.0**	**56478.0**	**0**	**--**
Equal speciation	5	-28294.7	56599.4	121.4	<2e-16 ***
Equal extinction	6	-28243.7	56499.4	21.4	0.001 ****
Equal dispersal	6	-28348.4	56708.9	230.8	<2e-16 ***

Supplementary Table 7. ESS values and Geweke's statistics of different parameters summarized across BAMM analyses of ten chronograms.

Statistics	**Statistical measures**	**number of shifts**	**Log prior**	**Log Likelihood**	**eventRate**	**acceptRate**
ESS	**min**	83	73	56	181	1616
	mean	140	143	83	265	2146
	max	186	185	121	330	2818
Geweke's statistics	**# of trees p > 0.05**	7	7	9	7	7

Supplementary Table 8. The results of linear regression analyses where the dependent variable was BAMM's net diversification or net speciation rate and the explanatory variable was net diversification rate inferred using the MS approach. ε = relative extinction rate.

MS estimates as explanatory variables	Statistics based on BAMM's net diversification rate (dependent variable)		Statistics based on BAMM's speciation rate (dependent variable)	
	Adjusted R^2	P-value	Adjusted R^2	P-value
stem ages & ε = 0	0.51	9.18E-15	0.45	9.17E-13
stem ages & ε = 0.5	0.50	2.42E-14	0.45	1.63E-12
stem ages & ε = 0.9	0.45	1.26E-12	0.41	2.47E-11
crown ages & ε = 0	0.60	2.68E-18	0.53	2.28E-15
crown ages & ε = 0.5	0.59	4.87E-18	0.52	3.27E-15
crown ages & ε = 0.9	0.55	3.48E-16	0.49	5.51E-14

Legends for supplementary data

Supplementary Data 1. (Separate file).
Data matrices of GenBank accession numbers of newly sequenced taxa, character states used for analyses of character evolution and taxon sampling statistics used in this study. The GenBank accession numbers are depicted for LSU sequences of 1213 newly sequenced species. The character state coding of cap presence/absence, fruiting body morphology, substrate preference and geographic distributions for 5,284 species is given.

Supplementary Data 2. (Separate file). Comparison of results of different molecular dating analyses. The inferred ages of seven clades (Agaricales, Boletales, Agaricomycetidae, Agaricomycetes, most recent common ancestor of Agaricomycetes and Dacrymycetes, Agaricomycotina) were compared with the estimates of two previous studies and five analyses of the present study (three methods r8s, mcmctree and a 2-stage Bayesian approach and three calibration schemes) to assess the impact of alternative placements of fossil calibration points.

Supplementary Data 3. (Separate file). Transition rate matrices of ancestral character state reconstruction (ASR) analyses and results of the ASR of fungal substrate preference.

Supplementary Data 4. (Separate file). Speciation, extinction and diversification rates through time obtained by iteratively removing orders and higher level clades from the phylogeny. Different colors represent the ten chronograms analyzed. Lines are median rates and color density denotes the 80% Bayesian credible regions on the distribution of rates. For each plot, the upper row (A) shows the rates calculated for the given clade, the lower (B) shows rates calculated for the entire tree, with the given clade deleted.

Supplementary Data 5. (Separate file). List of highly supported core shifts that are congruent across multiple trees. Statistics of the shifts (Posterior probability, Prior to posterior odds ratio, Speciation rate change etc.) are given. Mean values are the average across the trees containing a core shift.

Supplementary Data 6. (Separate file). Lineages through time (LTT) plots for the clades containing highly supported core shifts. LTT plots were generated from branches subtending a congruent core shift with the ltt.plot function in the R package ape v.4.1. Dashed red line represents the log linear (exponential) change of the number of lineages based on the extant species number. If the slope of the inferred changes in lineage number is higher or lower than that of the dashed red line, the number of lineages increased faster or slower than it is expected.

Supplementary Data 7. (Separate file). Parameters and detailed results of BayesTraits and BiSSE analyses. The mean and the variance of the estimated transition rates are given for the Maximum Likelihood and Bayesian MCMC analyses of BayesTraits and BiSSE analyses. Furthermore, the hyperprior intervals are given for Bayesian analyses in BayesTraits. Results of the model tests are also included: log likelihood values, bayes factors, likelihood ratio tests.

References

1. Rodréguez-Ezpeleta, N. *et al.* Detecting and overcoming systematic Errors in genome-scale phylogenies. *Syst. Biol.* **56,** 389–399 (2007).
2. Dentinger, B. T. M. *et al.* Tales from the crypt: Genome mining from fungarium specimens improves resolution of the mushroom tree of life. *Biol. J. Linn. Soc.* **117,** 11–32 (2016).
3. Zhao, R.-L. *et al.* A six-gene phylogenetic overview of Basidiomycota and allied phyla with estimated divergence times of higher taxa and a phyloproteomics perspective. *Fungal Divers.* **84,** 43–74 (2017).
4. Hibbett, D. S. A phylogenetic overview of the Agaricomycotina. *Mycologia* **98,** 917–925 (2006).
5. Nagy, L. G. *et al.* Comparative genomics of early-diverging mushroom-forming fungi provides insights into the origins of lignocellulose decay capabilities. *Mol. Biol. Evol.* **33,** 959–970 (2016).
6. Kohler, A. *et al.* Convergent losses of decay mechanisms and rapid turnover of symbiosis genes in mycorrhizal mutualists. *Nat. Genet.* **47,** 410–415 (2015).
7. Floudas, D. *et al.* The Paleozoic Origin of Enzymatic Lignin Decomposition Reconstructed from 31 Fungal Genomes. *Science (80-.).* **336,** 1715–1719 (2012).
8. Hibbett, D. S. *et al.* in *Systematics and Evolution* 373–429 (Springer Berlin Heidelberg, 2014). doi:10.1007/978-3-642-55318-9_14
9. Matheny, B. P. *et al.* Contributions of rpb2 and tef1 to the phylogeny of mushrooms and allies (Basidiomycota, Fungi). *Mol. Phylogenet. Evol.* **43,** 430–451 (2007).
10. Binder, M., Larsson, K.-H., Matheny, P. B. & Hibbett, D. S. Amylocorticiales ord. nov. and Jaapiales ord. nov.: Early diverging clades of Agaricomycetidae dominated by corticioid forms. *Mycologia* **102,** 865–880 (2010).
11. Binder, M. *et al.* Phylogenetic and phylogenomic overview of the Polyporales. *Mycologia* **105,** 1350–1373 (2013).
12. Binder, M. *et al.* The phylogenetic distribution of resupinate forms across the major clades of mushroom-forming fungi (Homobasidiomycetes). *Syst. Biodivers.* **3,** 113–157 (2005).
13. Justo, A. *et al.* A revised family-level classification of the Polyporales (Basidiomycota). *Fungal Biol.* **121,** 798–824 (2017).
14. Matheny, P. B. *et al.* Major clades of Agaricales: a multilocus phylogenetic overview. *Mycologia* **98,** 982–995 (2006).
15. Floudas, D. *et al.* Evolution of novel wood decay mechanisms in Agaricales revealed by the genome sequences of Fistulina hepatica and Cylindrobasidium torrendii. *Fungal Genet. Biol.* **76,** 78–92 (2015).
16. Nagy, L. G. *et al.* Latent homology and convergent regulatory evolution underlies the repeated emergence of yeasts. *Nat. Commun.* **5,** 4471 (2014).
17. Binder, M. & Hibbett, D. S. Molecular systematics and biological diversification of Boletales. *Mycologia* **98,** 971–981 (2006).
18. Gnerre, S. *et al.* High-quality draft assemblies of mammalian genomes from massively parallel sequence data. *Proc. Natl. Acad. Sci.* **108,** 1513–1518 (2011).
19. Martin, J. *et al.* Rnnotator: an automated de novo transcriptome assembly pipeline from stranded RNA-Seq reads. *BMC Genomics* **11,** 663 (2010).
20. Grigoriev, I. V *et al.* MycoCosm portal: Gearing up for 1000 fungal genomes. *Nucleic Acids Res.* **42,** (2014).

21. Lidgard, S. & Crane, P. R. Quantitative analyses of the early angiosperm radiation. *Nature* **331,** 344–346 (1988).
22. Smith, J. F. *et al.* The Emergence of Earliest Angiosperms May be Earlier than Fossil Evidence Indicates. *Syst. Bot.* **42,** 1–13 (2017).
23. Lu, Y., Ran, J., Guo, D., Yang, Z. & Wang, X. Phylogeny and Divergence Times of Gymnosperms Inferred from Single-Copy Nuclear Genes. *PLoS One* **9,** 1–15 (2014).
24. Goldberg, E. E., Lancaster, L. T. & Ree, R. H. Phylogenetic Inference of Reciprocal Effects between Geographic Range Evolution and Diversification. *Syst. Biol.* **60,** 451–465 (2011).
25. Morin, E. *et al.* Genome sequence of the button mushroom Agaricus bisporus reveals mechanisms governing adaptation to a humic-rich ecological niche. *Proc. Natl. Acad. Sci.* **109,** 17501–17506 (2012).
26. Wolfe, B. E., Kuo, M. & Pringle, A. *Amanita thiersii* is a saprotrophic fungus expanding its range in the United States. *Mycologia* **104,** 22–33 (2012).
27. Collins, C. *et al.* Genomic and proteomic dissection of the ubiquitous plant pathogen, armillaria mellea: Toward a new infection model system. *J. Proteome Res.* **12,** 2552–2570 (2013).
28. Floudas, D. *et al.* The Paleozoic origin of enzymatic lignin decomposition reconstructed from 31 fungal genomes. *Science* **336,** 1715–9 (2012).
29. Riley, R. *et al.* Extensive sampling of basidiomycete genomes demonstrates inadequacy of the white-rot/brown-rot paradigm for wood decay fungi. *Proc. Natl. Acad. Sci.* **111,** 9923–9928 (2014).
30. Fernandez-Fueyo, E. *et al.* Comparative genomics of Ceriporiopsis subvermispora and Phanerochaete chrysosporium provide insight into selective ligninolysis. *Proc. Natl. Acad. Sci.* **109,** 5458–5463 (2012).
31. Stajich, J. E. *et al.* Insights into evolution of multicellular fungi from the assembled chromosomes of the mushroom Coprinopsis cinerea (Coprinus cinereus). *Proc. Natl. Acad. Sci. U. S. A.* **107,** 11889–11894 (2010).
32. Janbon, G. *et al.* Analysis of the Genome and Transcriptome of Cryptococcus neoformans var. grubii Reveals Complex RNA Expression and Microevolution Leading to Virulence Attenuation. *PLoS Genet.* **10,** e1004261 (2014).
33. Tang, J. D. *et al.* Short-read sequencing for genomic analysis of the brown rot fungus Fibroporia radiculosa. *Appl. Environ. Microbiol.* **78,** 2272–2281 (2012).
34. Doré, J. *et al.* Comparative genomics, proteomics and transcriptomics give new insight into the exoproteome of the basidiomycete Hebeloma cylindrosporum and its involvement in ectomycorrhizal symbiosis. *New Phytol.* **208,** 1169–1187 (2015).
35. Olson, Å. *et al.* Insight into trade-off between wood decay and parasitism from the genome of a fungal forest pathogen. *New Phytol.* **194,** 1001–1013 (2012).
36. Martin, F. *et al.* The genome of Laccaria bicolor provides insights into mycorrhizal symbiosis. *Nature* **452,** 88–92 (2008).
37. Aylward, F. O. *et al.* Leucoagaricus gongylophorus Produces Diverse Enzymes for the Degradation of Recalcitrant Plant Polymers in Leaf-Cutter Ant Fungus Gardens. *Appl. Environ. Microbiol.* **79,** 3770–3778 (2013).
38. Mondego, J. M. C. *et al.* A genome survey of Moniliophthora perniciosa gives new insights into Witches' Broom Disease of cacao. *BMC Genomics* **9,** (2008).
39. Miettinen, O. *et al.* Draft Genome Sequence of the White-Rot Fungus Obba rivulosa 3A-

2. *Genome Announc.* **4,** 00976-16 (2016).
40. Wawrzyn, G. T., Quin, M. B., Choudhary, S., López-Gallego, F. & Schmidt-Dannert, C. Draft Genome of Omphalotus olearius Provides a Predictive Framework for Sesquiterpenoid Natural Product Biosynthesis in Basidiomycota. *Chem. Biol.* **19,** 772–783 (2012).
41. Ohm, R. A. *et al.* Genomics of wood-degrading fungi. *Fungal Genet. Biol.* **72,** 82–90 (2014).
42. Hori, C. *et al.* Analysis of the Phlebiopsis gigantea Genome, Transcriptome and Secretome Provides Insight into Its Pioneer Colonization Strategies of Wood. *PLoS Genet.* **10,** (2014).
43. Zuccaro, A. *et al.* Endophytic life strategies decoded by genome and transcriptome analyses of the mutualistic root symbiont Piriformospora indica. *PLoS Pathog.* **7,** (2011).
44. Castanera, R. *et al.* Transposable Elements versus the Fungal Genome: Impact on Whole-Genome Architecture and Transcriptional Profiles. *PLoS Genet.* **12,** 1–27 (2016).
45. Alfaro, M. *et al.* Comparative and transcriptional analysis of the predicted secretome in the lignocellulose-degrading basidiomycete fungus Pleurotus ostreatus. *Environ. Microbiol.* **18,** 4710–4726 (2016).
46. Martinez, D. *et al.* Genome, transcriptome, and secretome analysis of wood decay fungus *Postia placenta*supports unique mechanisms of lignocellulose conversion. *Proc. Natl. Acad. Sci.* **106,** 1954–1959 (2009).
47. Wibberg, D. *et al.* Establishment and interpretation of the genome sequence of the phytopathogenic fungus Rhizoctonia solani AG1-IB isolate 7/3/14. *J. Biotechnol.* **167,** 142–155 (2013).
48. Min, B. *et al.* Genome sequence of a white rot fungus Schizopora paradoxa KUC8140 for wood decay and mycoremediation. *J. Biotechnol.* **211,** 42–43 (2015).
49. Eastwood, D. C. *et al.* The Plant Cell Wall-Decomposing Machinery Underlies the Functional Diversity of Forest Fungi. *Science (80-.).* **333,** 762–765 (2011).
50. Bao, D. *et al.* Sequencing and Comparative Analysis of the Straw Mushroom (Volvariella volvacea) Genome. *PLoS One* **8,** (2013).
51. Smith, S. Y., Currah, R. S. & Stockey, R. A. Cretaceous and Eocene poroid hymenophores from Vancouver Island, British Columbia. *Mycologia* **96,** 180–186 (2004).
52. Fleischmann, A., Krings, M., Mayr, H. & Agerer, R. Structurally preserved polypores from the Neogene of North Africa: Ganodermites libycus gen. et sp. nov. (Polyporales, Ganodermataceae). *Rev. Palaeobot. Palynol.* **145,** 159–172 (2007).
53. Hibbett, D. S., Grimaldi, D. & Donoghue, M. J. Fossil mushrooms from Miocene and Cretaceous ambers and the evolution of homobasidiomycetes. *Am. J. Bot.* **84,** 981–991 (1997).
54. Poinar, G. O. & Buckley, R. Evidence of mycoparasitism and hypermycoparasitism in Early Cretaceous amber. *Mycol. Res.* **111,** 503–506 (2007).
55. Poinar, G. Bird's nest fungi (Nidulariales: Nidulariaceae) in Baltic and Dominican amber. *Fungal Biol.* **118,** 325–329 (2014).
56. Lepage, B. A., Currah, R. S., Stockey, R. A. & Rothwell, G. W. Fossil ectomycorrhizae from the middle Eocene. *Am. J. Bot.* **84,** 410–412 (1997).
57. Duringer, P. *et al.* The first fossil fungus gardens of Isoptera: Oldest evidence of symbiotic termite fungiculture (Miocene, Chad basin). *Naturwissenschaften* **93,** 610–615 (2006).

58. Knobloch, E. & Kotlaba, F. Trametites eocenicus, a new fossil polypore from the Bohemian Eocene. *Czech Mycol.* **47,** 207–214 (1994).